Probabilistic Engineering Mechanics 85 (2026) 103982

Contents lists available at ScienceDirect

Probabilistic Engineering Mechanics

journal homepage: www.elsevier.com/locate/probengmech

In-sample versus ensemble optimisation of tuned mass dampers for structures with uncertainties

Sudip Chowdhury *, Sondipon Adhikari

Infrastructure and Environment, James Watt School of Engineering, The University of Glasgow, Glasgow, Scotland, United Kingdom

ARTICLE INFO

Keywords:
Tuned mass damper
Frequency uncertainty
Robust design
Ensemble optimisation
Monte Carlo simulation
Vibration control

ABSTRACT

Classical tuned mass damper (TMD) design assumes precisely known structural properties, but no systematic framework exists when the primary structure is uncertain due to material variability, construction tolerances, or environmental factors. This paper introduces a conceptual dichotomy in robust TMD design: in-sample optimisation, which determines parameters conditionally for individual structural realisations, versus ensemble optimisation, which seeks distributional robustness across the entire population of uncertain structures. This represents a fundamental departure from existing approaches, which treat uncertainty as a post-design consideration rather than embedding it within the optimisation formulation itself. A probabilistic framework is developed in which structural natural frequency is modelled as a random variable, and dynamic responses are characterised through closed-form analytical expressions for mean and variance, validated against Monte Carlo simulation. The in-sample approach applies fixed-point theory to each realisation and aggregates the resulting parameter distributions. The ensemble approach enforces equal-mean constraints on fixed-point frequencies across the uncertainty distribution and minimises response variance. Comparative analyses in both frequency and time domains demonstrate that while conventional deterministic TMDs remain sensitive to detuning, both proposed strategies effectively suppress resonance amplification. The ensemble design achieves superior performance, reducing maximum structural displacement by 21.50% relative to conventional TMD, compared to 19.32% for in-sample design. Beyond parameter optimisation, this work establishes in-sample versus ensemble as a transferable design philosophy for vibration control under uncertainty, with direct implications for adaptive versus mass-produced damper systems in engineering practice.

1. Introduction

Excessive vibration in engineering structures subjected to dynamic loading, such as wind, earthquakes, ocean waves, traffic loads, and machinery induced excitations, remains a critical concern in structural design and serviceability [1]. These dynamic actions often induce resonance phenomena, where even relatively small external forces can generate large structural responses when their frequencies coincide with the natural frequencies of the system [2]. Such amplified vibrations may lead to progressive fatigue damage, degradation of structural components, and, in extreme cases, structural failure [3]. In addition to safety concerns, excessive vibration adversely affects serviceability by causing discomfort to occupants [4], impairing the functionality of sensitive equipment, and increasing maintenance and operational costs [5]. To mitigate these effects, a range of vibration control strategies has been developed, including passive, active, and semi-active control systems [6]. Among these, passive devices are particularly attractive due to their simplicity, reliability, and independence from external power sources. The tuned mass damper (TMD) is one of the most widely adopted passive control devices [7], consisting of an auxiliary mass attached to the primary structure through a spring-damper mechanism [8]. When properly tuned, the TMD interacts dynamically with the structure, enabling effective transfer and dissipation of vibrational energy, particularly near resonance conditions, thereby reducing peak structural response [9].

Classical TMD design approaches are predominantly deterministic, assuming that the dynamic properties of the primary structure, especially its natural frequency, are precisely known and remain constant [10]. Under this assumption, optimal tuning conditions [11] have been derived to minimise the maximum steady state response, typically by equalising the amplitudes of resonance peaks in the frequency response function [12]. While these formulations provide useful and widely accepted design guidelines, they do not account for the inherent variability present in real

* Corresponding author.
E-mail address: Sudip.Chowdhury@glasgow.ac.uk (S. Chowdhury).

https://doi.org/10.1016/j.probengmech.2026.103982
Received 19 May 2026; Received in revised form 24 June 2026; Accepted 28 June 2026
Available online 2 July 2026

world structures [13]. In practice, structural properties are affected by uncertainties arising from material heterogeneity, construction tolerances, modelling simplifications, environmental influences such as temperature and humidity, and long-term effects including ageing and damage accumulation [14]. These uncertainties can lead to variations in stiffness, mass distribution, and damping characteristics, ultimately causing shifts in the natural frequency of the structure [15]. As a consequence, a TMD designed under deterministic assumptions may become detuned from the primary system, resulting in reduced effectiveness or even amplification of structural response near resonance [16]. This sensitivity to parameter uncertainty highlights a fundamental limitation of conventional design methods and underscores the importance of developing robust design strategies that explicitly incorporate uncertainty into the analysis and optimisation process [17].

In the context of vibration control, the H_∞ optimisation framework provides a rigorous basis for designing systems that minimise the worst-case dynamic amplification over a prescribed frequency range [18]. Unlike classical tuning methods that focus on specific resonance conditions, the H_∞ approach seeks to minimise the supremum [19] of the frequency response function, thereby ensuring robust performance against variations in excitation frequency and system parameters [20]. For TMD design, this corresponds to minimising the peak magnitude of the transfer function between the external excitation and the structural response, resulting in a flattened frequency response with reduced sensitivity to detuning [21]. Although this approach is inherently conservative due to its focus on worst-case responses, it provides enhanced reliability and robustness under uncertain conditions [22]. The concept of limiting the maximum response plays a central role in robust vibration control and forms a theoretical foundation for many modern optimisation strategies [23]. In this paper, this perspective is extended by combining peak-response minimisation with statistical measures, allowing both the worst-case behaviour and the overall variability of the response to be addressed simultaneously.

Recent advances in probabilistic structural dynamics and uncertainty quantification have enabled the systematic incorporation of randomness into the modelling and analysis of vibration control systems [24]. In this framework, uncertain parameters, such as the natural frequency of the primary structure, are treated as random variables characterised by probability distributions [25]. This probabilistic representation allows the structural response to be described in terms of statistical measures, including the mean, variance, and higher order moments, which provide a more clear understanding of system behaviour under uncertainty [26]. The mean response reflects the expected performance of the structure, while the variance quantifies the degree of dispersion and reliability [27]. Monte Carlo simulation (MCS) is widely employed for evaluating stochastic responses due to its flexibility and applicability to complex systems [28]. The use of advanced sampling techniques, such as Latin hypercube sampling, enhances the efficiency and convergence of MCS by ensuring a more uniform exploration of the uncertainty space [29]. In addition, numerical quadrature methods offer accurate and computationally efficient alternatives for evaluating statistical moments when the probability distribution is well defined [30]. These probabilistic tools form the foundation for developing robust design methodologies that aim to achieve not only optimal performance but also reduced sensitivity to uncertainty.

Recent developments in passive vibration control systems have demonstrated that the performance limitations of classical tuned mass dampers under structural uncertainties can be improved through advanced absorber configurations. In particular, inerter-based tuned mass damper systems have attracted significant attention due to their ability to generate enhanced apparent inertia and improved energy redistribution without substantially increasing the physical mass of the absorber [31,32]. These systems have demonstrated superior vibration mitigation and improved robustness against detuning effects under uncertain structural and excitation conditions [33,34]. Similarly, multiple tuned mass damper systems connected in series or parallel configurations have been proposed to broaden the effective operational bandwidth of vibration absorbers by distributing the control mechanism across multiple frequencies. Such configurations reduce the sensitivity of the control system to parameter variations and improve vibration suppression under broadband dynamic excitations [35]. In addition, friction-based tuned mass dampers [36] have emerged as an effective nonlinear vibration mitigation strategy by introducing Coulomb friction induced energy dissipation. These systems can suppress large amplitude oscillations and improve damping performance under transient and stochastic loading conditions [37,38]. Advanced vibration control systems provide improved physical vibration mitigation mechanisms compared with conventional TMDs; however, the majority of existing studies primarily focus on developing new absorber configurations or improving deterministic tuning performance. Comparatively limited attention has been devoted to establishing unified optimisation philosophies capable of systematically distinguishing between conditional optimality for individual structural realisations and distributional robustness across uncertain structural populations. Consequently, the uncertainty-aware optimisation framework proposed in this paper may provide a useful analytical foundation for future extensions to inerter-based, multiple, and nonlinear friction-based vibration absorbers operating under structural uncertainties.

Although several previous studies have investigated robust or reliability based optimisation of tuned mass dampers under uncertainty, most existing approaches treat uncertainty within a single optimisation framework and primarily focus on improving robustness through stochastic or reliability based parameter tuning. In these formulations, uncertainty is generally incorporated as a perturbation within the optimisation process, while the underlying optimisation philosophy itself remains unchanged. In contrast, this paper introduces a conceptual distinction between two fundamentally different optimisation strategies under uncertainty: in-sample optimisation and ensemble-based optimisation. The in-sample approach determines optimal damper parameters conditionally for each realisation of the uncertain structure, whereas the ensemble-based approach seeks a single robust design by optimising the response statistics across the entire uncertainty distribution. This distinction establishes a systematic framework for differentiating between conditional optimality and distributional robustness in vibration control systems under uncertainty. Despite these developments, a unified analytical framework capable of systematically comparing conditional and distributional optimisation philosophies for tuned mass dampers under uncertainty remains limited in the existing literature. To address this research gap, this paper develops closed-form analytical formulations for stochastic structural responses and establishes uncertainty-informed optimal tuning strategies using both in-sample and ensemble-based formulations. The effectiveness of the proposed methodologies is investigated through frequency domain and time domain analyses. Analytical solutions are derived for the coupled stochastic system, while Monte Carlo simulations are employed to validate the proposed formulations and quantify the stochastic behaviour. The performance of the proposed designs is evaluated in terms of vibration reduction, response variability, and robustness under uncertainty. Comparisons with conventional deterministic tuned mass damper designs are also presented to highlight the advantages of incorporating uncertainty directly within the optimisation framework.

The remainder of this paper is organised as follows. Section 2 presents the formulation of the structural model and the governing equations of motion. Section 3 introduces the probabilistic representation of uncertainty and develops the associated stochastic response measures. Section 3.2 establishes the framework for determining optimal damper parameters under structural uncertainty. Sections 4 and 5 present the in-sample and ensemble-based optimal design methodologies, respectively. Section 6 provides a detailed discussion and comparison of the resulting design parameters. Section 7 presents the dynamic response analysis in both the frequency and time domains, along with comprehensive numerical results. Finally, concluding remarks are provided in Section 8.

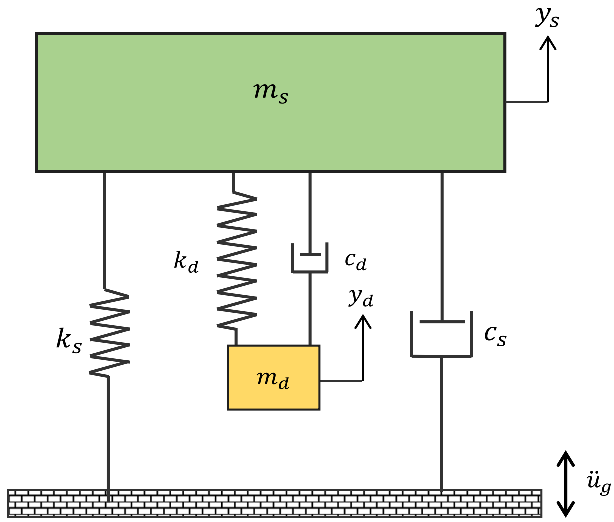

Fig. 1. A tuned mass damper is installed at the top of a structure to control its vibration.

2. Structural model and equations of motion

Fig. 1 illustrates a single-degree-of-freedom primary structure equipped with a tuned mass damper and subjected to base excitation. The coupled structure-damper system is represented by an equivalent two-degree-of-freedom lumped-parameter model. The governing equations of motion are formulated in terms of relative displacements with respect to the ground motion, and harmonic steady-state solutions are subsequently employed to derive the frequency response functions used in the stochastic analysis and optimisation framework presented in the following sections. m_s, $c_s = 2m_s\xi_s\omega_s$, and $k_s = m_s\omega_s^2$ define the mass, damping, and stiffness of the SDOF system. ω_s defines the frequency of the SDOF system. ξ_s defines the damping ratio of the SDOF system. m_d defines the mass fo the damper. $k_d = m_d\omega_d^2$ defines the stiffness of the damper. $c_d = 2m_d\xi_d\omega_d$ defines the damping of the damper. $\ddot{u}_g$ is applied at the base of the controlled SDOF system. Accordingly, the deflections are generated in the controlled SDOF systems. $y_s(t)$ defines the absolute displacement of the structure mass m_s, $y_d(t)$ defines the displacement of the damper's mass m_d, and $u_g(t)$ defines the ground displacement of the base excitation. The relative displacements of the structure and damper are derived

$$u_s = y_s - u_g \quad \text{and} \quad u_d = y_d - y_s \tag{1}$$

Since the internal forces in springs and dampers rely on the deformation between two points rather than their absolute positions in space, relative displacement is required. By treating the acceleration of the ground as an effective inertial force acting on a fixed-base system, it also makes the equations of motion simpler. Lagrange's equation is applied to derive the governing equations of motion of the controlled SDOF system using the energy method, and the equation of motion is derived as

$$\begin{aligned} &m_s\ddot{u}_s + c_s\dot{u}_s + k_s u_s - c_d\dot{u}_d - k_d u_d = -m_s\ddot{u}_g \\ &m_d\ddot{u}_s + m_d\ddot{u}_d + c_d\dot{u}_d + k_d u_d = -m_d\ddot{u}_g \end{aligned} \tag{2}$$

Due to the presence of base excitation, the displacement responses of SDOF system and damper are developed. Accordingly, the displacement responses are considered as $u_s = U_s e^{\mathrm{i}\omega t}$ and $u_d = U_d e^{\mathrm{i}\omega t}$. The ground acceleration is considered as $\ddot{u}_g = U_g e^{\mathrm{i}\omega t}$. These steady state responses are substituted in Eq. (2) to derive the transfer matrix. The matrix is derived as

$$\begin{bmatrix} -r^2 + 2\,\mathrm{i}r\nu\xi_s + \nu^2 & -2\,\mathrm{i}r\mu_d\Omega_d\xi_d - \mu_d\Omega_d^2 \\ -r^2\mu_d & -r^2\mu_d + 2\,\mathrm{i}r\mu_d\Omega_d\xi_d + \mu_d\Omega_d^2 \end{bmatrix} \begin{Bmatrix} U_s \\ U_d \end{Bmatrix} = \begin{bmatrix} -1 \\ -\mu_d \end{bmatrix} \left(\frac{U_g}{\omega_{s0}^2} \right) \tag{3}$$

where $r = \omega/\omega_{s0}$ defines the random frequency ratio. $\mu_d = m_d/m_s$ defines the ratio of damper mass and the structure. $\Omega_d = \omega_d/\omega_{s0}$ defines the frequency ratio of damper. ξ_d defines the damping ratio of the damper. The relative displacement of the SDOF system is derived as

$$H_s = \left(\frac{U_s}{U_g} \right) \omega_{s0}^2 = \frac{\mu_d\Omega_d^2 - r^2 + \Omega_d^2 + \mathrm{i}\left(2r\mu_d\Omega_d\xi_d + 2\Omega_d\xi_d r\right)}{\Delta} \tag{4}$$

The relative displacement of the damper is derived as

$$H_d = \left(\frac{U_d}{U_g} \right) \omega_{s0}^2 = \frac{-\nu\left(2\,\mathrm{i}r\xi_s + \nu\right)}{\Delta} \tag{5}$$

The closed-form expression for Δ is derived as

$$\Delta = \begin{array}{c} 4\nu r^2\xi_d\xi_s\Omega_d + \mu_d r^2\Omega_d^2 + \nu^2 r^2 - \nu^2\Omega_d^2 - r^4 + r^2\Omega_d^2 \\ +\mathrm{i}\left(2\mu_d r^3\xi_d\Omega_d - 2\nu^2 r\xi_d\Omega_d + 2\nu r^3\xi_s - 2\nu r\xi_s\Omega_d^2 + 2r^3\xi_d\Omega_d\right) \end{array} \tag{6}$$

Initially, the uncertainty is considered at the natural frequency of the main structure. Accordingly, it has been considered that the natural frequency of the primary structure is random. The natural frequency is derived as

$$\omega_s = \nu\omega_{s0} \quad \text{and} \quad \nu^2 = (1 + \varepsilon\chi) \tag{7}$$

where ν defines the frequency random factor. χ is a random variable with a given probability distribution function. ϵ defines the statistical scatter which scales the intensity of the stochastic perturbation. It should be noted that the natural frequency of the primary structure is assumed to be uncertain in the present study to represent the variability encountered in practical engineering systems. In reality, structural properties are influenced by uncertainties in material characteristics, manufacturing and construction tolerances, boundary-condition imperfections, environmental effects, operational loading, ageing, deterioration, and damage accumulation. These factors may alter the effective stiffness and mass distribution of the structure, leading to variability in its natural frequency. Since the vibration mitigation performance of a tuned mass damper is highly sensitive to frequency mistuning, even small deviations in the structural natural frequency may result in significant reductions in control effectiveness. The uncertainty is therefore modelled through the primary structural natural frequency, which serves as an effective parameter that captures the combined influence of the underlying physical uncertainties in a mathematically tractable manner. From an engineering perspective, the objective is not to design a different TMD for every possible structural realisation, but rather to determine a robust set of absorber parameters capable of maintaining satisfactory performance across a population of uncertain structures. In the present study, the uncertainty domain is represented through 1000 structural realisations generated from the prescribed probability distribution, thereby simulating a population of nominally similar structures with uncertain dynamic properties. Consequently, the ensemble-based optimisation framework seeks a single TMD design that remains effective across all considered structural realisations, thereby enhancing practical applicability and robustness against uncertainty-induced frequency detuning.

3. Uncertainty modelling and stochastic response evaluation

Since the effectiveness of tuned mass dampers is highly sensitive to structural frequency variations, it is necessary to incorporate uncertainty directly into the dynamic response formulation. In this section, the uncertain structural frequency is modelled probabilistically, and the corresponding stochastic response quantities are evaluated through analytical formulations and Monte Carlo simulations. The developed framework enables systematic assessment of both the mean behaviour and response variability of the controlled system under uncertainty.

3.1. Uncertainty modelling

The values of the mean and standard deviation for χ are considered as zero and 1. Accordingly, the probability density function [39] is obtained as

$$P_{\chi}(\chi) = \frac{1}{2\sqrt{3}} \quad \text{and} \quad -\sqrt{3} \leq \chi \leq \sqrt{3} \tag{8}$$

In this paper, a uniform probability distribution is adopted for the uncertain structural natural frequency in order to represent bounded parametric uncertainty in the absence of precise statistical information regarding the actual distribution of the structural properties. In many practical engineering applications, uncertainties associated with material variability, fabrication tolerances, environmental conditions, and boundary imperfections are often known only within admissible upper and lower bounds, while the exact probability density function remains unavailable. Under such conditions, the uniform distribution provides an unbiased representation by assigning equal probability to all admissible realisations within the prescribed uncertainty interval. The adopted formulation therefore enables systematic evaluation of the robustness and sensitivity of the proposed optimisation strategies across the entire uncertainty domain without introducing additional assumptions regarding the concentration of probability density around the nominal structural frequency. In particular, the uniform distribution avoids assigning preferential importance to structural realisations near the nominal frequency, thereby ensuring that the robustness of the proposed TMD optimisation framework is assessed over the complete admissible uncertainty range. It should be noted that the optimisation framework and the stochastic response evaluation presented in this study serve different purposes and are therefore based on different assumptions regarding the primary structural damping ratio. The classical fixed-point theory developed by Den Hartog is derived for an undamped primary structure ($\xi_s = 0$) and forms the basis for the closed-form determination of the optimal TMD tuning parameters. Consequently, the in-sample and ensemble-based optimisation frameworks employ the undamped fixed-point condition to preserve analytical tractability and maintain consistency with the established tuning methodology.

However, practical engineering structures invariably possess a finite amount of inherent damping arising from material hysteresis, joint friction, connection flexibility, and other energy dissipation mechanisms. Consequently, the objective of the present stochastic response analysis is not to determine the optimal absorber parameters, but rather to evaluate the practical performance and robustness of the optimised TMD designs under realistic operating conditions. For this reason, a non-zero primary structural damping ratio is considered during the response evaluation stage. Accordingly, the optimisation stage employs the classical undamped fixed-point formulation to determine the absorber parameters, whereas the stochastic response analysis incorporates structural damping to assess the effectiveness of the resulting designs in realistic uncertain structural systems.

Case 1: $\xi_s \neq 0$ **and** $\xi_d = 0$

Initially, the damping of the damper is considered zero, i.e., $\xi_d = 0$, to consider the worst case scenario. Accordingly, the transfer function of the dynamic response of the SDOF system is derived as

$$\begin{aligned} H_s(r,\chi)|_{\xi_d=0} &= \left(\frac{U_s}{U_g}\right)\omega_{s0}^2\Big|_{\xi_d=0} \\ &= \frac{\mu_d \Omega_d^2 - r^2 + \Omega_d^2}{\mu_d r^2 \Omega_d^2 + \nu^2\left(r^2 - \Omega_d^2\right) - r^4 + r^2\Omega_d^2 + \mathrm{i}\nu\left(2r^3\xi_s - 2r\xi_s\Omega_d^2\right)} \end{aligned} \tag{9}$$

Eq. (7) is substituted in Eq. (9). The stochastic response statistics are evaluated using Monte Carlo simulations in conjunction with the derived analytical transfer functions. Direct application of the stochastic variable transformation theorem to obtain the exact response probability density function becomes analytically difficult because the response expressions contain complicated rational functions of the uncertain structural frequency

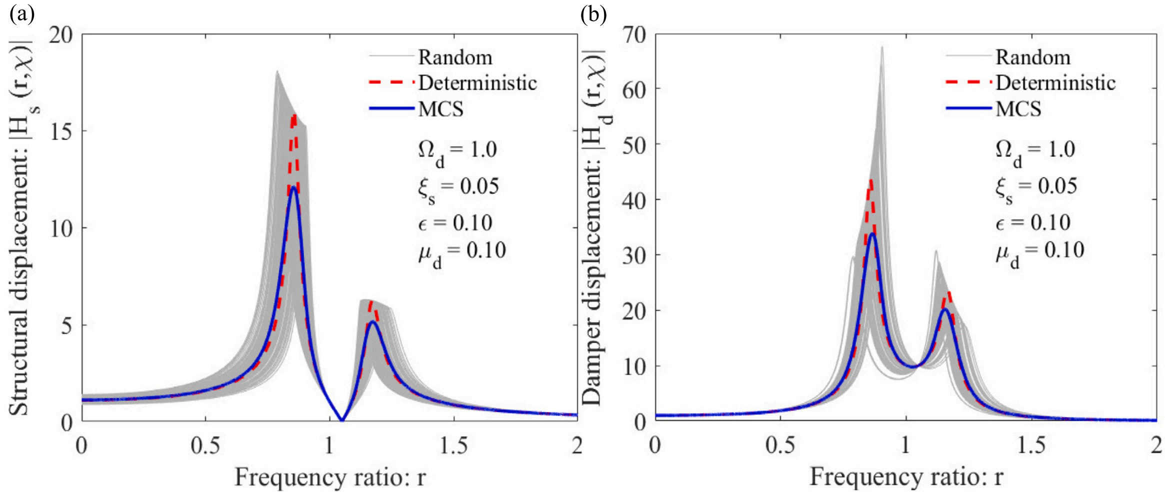

Fig. 2. The displacements of the (a) structure and (b) damper under stochasticity in primary structure parameters. (For interpretation of the references to colour in this figure legend, the reader is referred to the web version of this article.)

parameter over the full frequency range. Furthermore, the transformation between the uncertain parameter space and the response amplitude space is not generally guaranteed to be globally one-to-one, which may complicate analytical density reconstruction. Such transformations require particular care in probability-density reconstruction because non-bijective mappings may lead to difficulties in preserving the probability measure and accounting for all contributing pre-images of the transformation [40]. Therefore, the probabilistic response characteristics reported in this study are evaluated directly in the original random-variable space through Monte Carlo simulations. For each realisation of the uncertain structural frequency, the corresponding response amplitude is computed directly from the governing response function, thereby avoiding the need for an explicit transformation of the response probability density function and the associated difficulties related to probability-density reconstruction. The adopted sampling procedure spans the complete bounded uncertainty domain associated with the prescribed uniform distribution and is used to validate the analytical mean and variance predictions. In the Monte Carlo simulations, 1000 independent realisations of the random variable χ are generated according to the uniform probability distribution defined in Eq. (8). For each realisation, the corresponding frequency random factor is computed using Eq. (7), and the resulting deterministic response is evaluated through the derived analytical transfer functions. The stochastic response statistics are then obtained from the ensemble of all response realisations. Since the samples are generated over the complete support of the prescribed probability distribution, the Monte Carlo simulations provide a direct numerical propagation of the uncertainty and adequately represent the entire admissible uncertainty domain considered in this study. The Monte Carlo results are subsequently used to validate the analytical mean and variance expressions derived herein. The amplitude of the dynamic response of the SDOF system is derived as

$$|H_s(r,\chi)| = \sqrt{\frac{\mu_d^2\Omega_d^4 - 2\mu_d r^2\Omega_d^2 + 2\mu_d\Omega_d^4 + r^4 - 2r^2\Omega_d^2 + \Omega_d^4}{\begin{array}{c}\left(\varepsilon^2 r^4 - 2\varepsilon^2 r^2\Omega_d^2 + \Omega_d^4\varepsilon^2\right)\chi^2 \\ +\left(\begin{array}{c} 4\varepsilon\, r^6\xi_s^2 - 8\varepsilon\, r^4\xi_s^2\Omega_d^2 + 4\varepsilon\, r^2\xi_s^2\Omega_d^4 + 2\mu_d\varepsilon\, r^4\Omega_d^2 \\ -2\mu_d\varepsilon\, r^2\Omega_d^4 - 2\varepsilon\, r^6 + 4\varepsilon\, r^4\Omega_d^2 - 2\varepsilon\, r^2\Omega_d^4 + 2\varepsilon\, r^4 \\ -4\varepsilon\, r^2\Omega_d^2 + 2\Omega_d^4\varepsilon \end{array}\right)\chi \\ +\mu_d^2 r^4\Omega_d^4 - 2\mu_d r^6\Omega_d^2 + 2\mu_d r^4\Omega_d^4 + r^8 + 4r^6\xi_s^2 - 2r^6\Omega_d^2 - 8r^4\xi_s^2\Omega_d^2 \\ +2\mu_d r^4\Omega_d^2 - 2\mu_d r^2\Omega_d^4 - 2r^6 + 4r^4\Omega_d^2 - 2r^2\Omega_d^4 + r^4 - 2r^2\Omega_d^2 + \Omega_d^4 \\ +r^4\Omega_d^4 + 4r^2\xi_s^2\Omega_d^4 \end{array}}} \tag{10}$$

The damper decouples the primary structure from vibration at anti-resonance frequency region. The anti-resonance frequency is derived from the numerator of Eq. (9) and expressed as

$$r = \sqrt{\Omega_d^2\left(1+\mu_d\right)} \tag{11}$$

The transfer function of the dynamic response of the damper is derived as

$$\begin{aligned} H_d(r,\chi)|_{\xi_d=0} &= \left(\frac{U_d}{U_g}\right)\omega_{s0}^2\bigg|_{\xi_d=0} \\ &= \frac{2\,\mathrm{i}r\nu\xi_s + \nu^2}{\mu_d r^2\Omega_d^2 + \nu^2\left(r^2-\Omega_d^2\right) - r^4 + r^2\Omega_d^2 + \mathrm{i}\nu\left(2\,r^3\xi_s - 2r\xi_s\Omega_d^2\right)} \end{aligned} \tag{12}$$

The amplitude of the dynamic response of the damper is derived as

$$|H_d(r,\chi)| = \sqrt{\frac{\chi^2\varepsilon^2 + \left(4\varepsilon r^2\xi_s^2 + 2\varepsilon\right)\chi + 4r^2\xi_s^2 + 1}{\begin{array}{c}\left(\varepsilon^2 r^4 - 2\varepsilon^2 r^2 \Omega_d^2 + \Omega_d^4\varepsilon^2\right)\chi^2 \\ +\left(\begin{array}{c} 4\varepsilon r^6\xi_s^2 - 8\varepsilon r^4\xi_s^2\Omega_d^2 + 4\varepsilon r^2\xi_s^2\Omega_d^4 + 2\mu_d\varepsilon r^4\Omega_d^2 \\ -2\mu_d\varepsilon r^2\Omega_d^4 - 2\varepsilon r^6 + 4\varepsilon r^4\Omega_d^2 - 2\varepsilon r^2\Omega_d^4 + 2\varepsilon r^4 \\ -4\varepsilon r^2\Omega_d^2 + 2\Omega_d^4\varepsilon\end{array}\right)\chi \\ +\mu_d^2 r^4\Omega_d^4 - 2\mu_d r^6\Omega_d^2 + 2\mu_d r^4\Omega_d^4 + r^8 + 4r^6\xi_s^2 - 2r^6\Omega_d^2 - 8r^4\xi_s^2\Omega_d^2 \\ +2\mu_d r^4\Omega_d^2 - 2\mu_d r^2\Omega_d^4 - 2r^6 + 4r^4\Omega_d^2 - 2r^2\Omega_d^4 + r^4 - 2r^2\Omega_d^2 + \Omega_d^4 \\ +r^4\Omega_d^4 + 4r^2\xi_s^2\Omega_d^4\end{array}}} \tag{13}$$

Fig. 2 illustrates the stochastic displacement responses of (a) the primary structure and (b) the attached damper under uncertainty in the structural frequency parameter, characterised by $\nu^2 = 1 + \varepsilon\chi$. The yellow curves represent individual random realisations, the black dashed line corresponds to the deterministic response, and the red curve shows the Monte Carlo simulation (MCS) mean response. For the primary structure (Fig. 2a), significant variability is observed near the resonance region. The random realisations exhibit a wide spread in peak amplitudes, indicating strong sensitivity of the structural response to uncertainty. The deterministic solution underestimates this variability and does not fully capture the stochastic amplification. In contrast, the MCS mean response provides a smoothed representation of the stochastic behaviour, lying below the extreme random peaks but above the deterministic curve near resonance. The anti-resonance dip is preserved, confirming the effectiveness of the TMD in suppressing vibration at the tuning frequency. For the damper response (Fig. 2b), a similar trend is observed, but with substantially higher peak amplitudes compared to the structure. This reflects the energy transfer mechanism of the tuned mass damper, where vibrational energy is absorbed and concentrated in the absorber. The stochastic spread is again pronounced around resonance, indicating that uncertainty significantly affects the damper motion. The MCS mean curve closely follows the central tendency of the random realisations, validating the probabilistic formulation. Overall, Fig. 2 demonstrates that uncertainty leads to substantial dispersion in both structural and damper responses, particularly near resonance. The comparison between random, deterministic, and MCS results highlights the necessity of stochastic analysis, as deterministic predictions alone are insufficient to characterise the true dynamic behaviour of the system. The mean responses of the structure is derived as

$$\begin{aligned}\overline{H_s(r)} &= \mathrm{E}\left[|H_s(r,\chi)|\right] = \int_{-\sqrt{3}}^{\sqrt{3}} |H_s(r,\chi)| P_\chi(\chi)\,\mathrm{d}\chi \\ &= \frac{\sqrt{3}\left(\begin{array}{c}\left(\left(\mu_d+1\right)\Omega_d^2 - r^2\right)\ln\left(\dfrac{G_5+\sqrt{G_3}\sqrt{\left(r^2-\Omega_d^2\right)^2\varepsilon^2}}{\sqrt{\left(r^2-\Omega_d^2\right)^2\varepsilon^2}}\right) \\ -\left(\left(\mu_d+1\right)\Omega_d^2 - r^2\right)\ln\left(-\dfrac{G_6-\sqrt{-G_4}\sqrt{\left(r^2-\Omega_d^2\right)^2\varepsilon^2}}{\sqrt{\left(r^2-\Omega_d^2\right)^2\varepsilon^2}}\right)\end{array}\right)}{6\sqrt{\left(r^2-\Omega_d^2\right)^2\varepsilon^2}}\end{aligned} \tag{14}$$

The closed-form expressions for G_3, G_4, G_5, and G_6 are listed in Appendix. In a similar manner, the mean response of the damper is derived as

$$\overline{H_d(r)} = \mathrm{E}\left[|H_d(r,\chi)|\right] = \int_{-\sqrt{3}}^{\sqrt{3}} |H_d(r,\chi)| P_\chi(\chi)\,\mathrm{d}\chi \tag{15}$$

The mean square value of the primary structure is derived as

$$\begin{aligned}\psi^2_{H_s(r)} &= \mathrm{E}\left[\left|H_s(r,\chi)\right|^2\right] = \int_{-\sqrt{3}}^{\sqrt{3}} \left|H_s(r,\chi)\right|^2 P_\chi(\chi)\,\mathrm{d}\chi \\ &= \frac{\sqrt{3}\left(\mu_d^2\Omega_d^4 - 2\mu_d r^2\Omega_d^2 + 2\Omega_d^4\mu_d + r^4 - 2r^2\Omega_d^2 + \Omega_d^4\right)N_s}{12\sqrt{-r^4\xi_s^2\varepsilon^2\left(r^2-\Omega_d^2\right)^3\left(r^2\xi_s^2 - \Omega_d^2\xi_s^2 + \mu_d\Omega_d^2 - r^2 + \Omega_d^2\right)}}\end{aligned} \tag{16}$$

The closed-form expression for N_s is listed in Appendix. The mean square value of the damper is derived as

$$\begin{aligned}\psi^2_{H_d(r)} &= \mathrm{E}\left[\left|H_d(r,\chi)\right|^2\right] = \int_{-\sqrt{3}}^{\sqrt{3}} \left|H_d(r,\chi)\right|^2 P_\chi(\chi)\,\mathrm{d}\chi \\ &= \frac{\begin{array}{c}2r^2\left(r^2-\Omega_d^2\left(\mu_d+1\right)\right)\left(\begin{array}{c}-2\varepsilon\left(r+\Omega_d\right)W r^2\left(r-\Omega_d\right)\arctan(Y) \\ -2\varepsilon\left(r+\Omega_d\right)W r^2\left(r-\Omega_d\right)\arctan(Z) \\ +V\left(\ln\left(G_1\right)-\ln\left(G_2\right)\right)\end{array}\right)\sqrt{3} \\ +12V\varepsilon\left(r-\Omega_d\right)\left(r+\Omega_d\right)\end{array}}{12V\varepsilon\left(r^6 - 3r^4\Omega_d^2 + 3r^2\Omega_d^4 - \Omega_d^6\right)}\end{aligned} \tag{17}$$

The closed-form expressions for W, Y, Z, G_1, G_2, and V are listed in Appendix. From the above expressions, the variance of the structural and damper responses as a function of the non-dimensional frequency r are obtained as

$$\sigma^2_{H_s(r)} = \psi^2_{H_s(r)} - \left(\overline{H_s(r)}\right)^2 \quad \text{and} \quad \sigma^2_{H_d(r)} = \psi^2_{H_d(r)} - \left(\overline{H_d(r)}\right)^2 \tag{18}$$

Fig. 3 presents the variance of the displacement responses for (a) the primary structure and (b) the absorber as functions of the frequency ratio. The results obtained from the analytical formulation are compared directly with those from Monte Carlo simulations (MCS), showing an almost

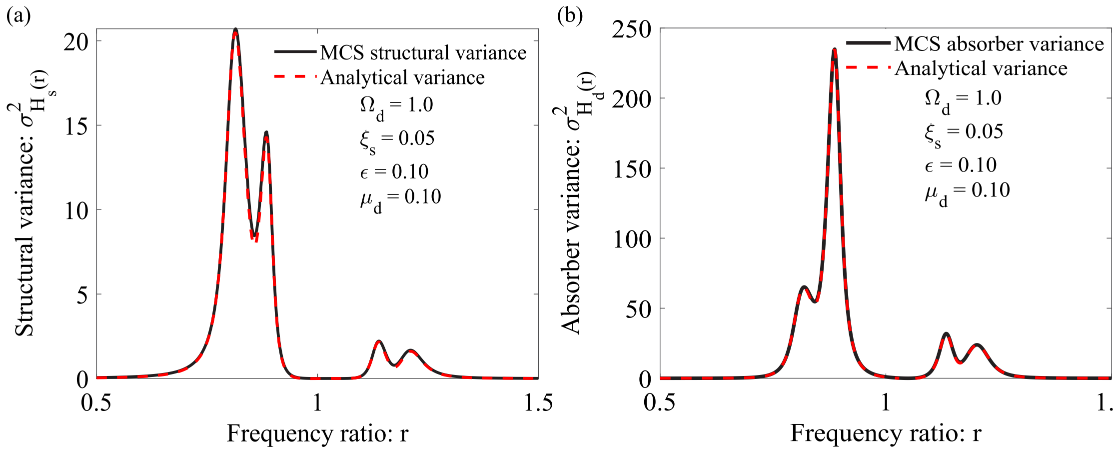

Fig. 3. The (a) structural and (b) damper variances versus frequency ratio. The analytical results are compared with the MCS results.

indistinguishable agreement across the entire frequency range. For the primary structure (Fig. 3a), the variance exhibits sharp peaks in the vicinity of the resonance region, indicating that the response is highly sensitive to uncertainty in the structural frequency. The presence of multiple peaks reflects the interaction between the primary system and the absorber, where energy redistribution leads to local amplification of variability. Away from resonance, the variance rapidly diminishes, suggesting that the influence of stochasticity becomes negligible in off-resonant regions. The excellent overlap between analytical and MCS curves confirms the accuracy of the derived closed-form expressions for predicting second-order response statistics. A similar behaviour is observed for the absorber response (Fig. 3b), although the magnitude of the variance is significantly higher. This is expected, as the absorber is designed to attract and dissipate vibrational energy, resulting in larger fluctuations under uncertain excitation conditions. The dominant peak near the primary resonance highlights that the absorber experiences the highest variability when it is most actively engaged in vibration mitigation. Secondary peaks are also present, corresponding to the coupled dynamics of the system. Overall, Fig. 3 demonstrates that the analytical variance expressions reliably capture the stochastic characteristics of both structural and absorber responses. The close agreement with MCS results validates the probabilistic framework and confirms that the derived formulations are capable of accurately quantifying uncertainty-induced variability in vibration control systems.

Case 2: $\xi_s = 0$ **and** $\xi_d \neq 0$

The damping of the primary structure is considered zero instead of damping of the damper. The structure is oscillating at the tuned frequency. The amount of dissipated energy is calibrated in this manner. The transfer function of the displacement response of the primary structure is derived as

$$\begin{aligned} H_s(r,\chi)|_{\xi_s=0} &= \left(\frac{U_s}{U_g}\right)\omega_{s0}^2\bigg|_{\xi_s=0} \\ &= \frac{\mu_d\Omega_d^2 - r^2 + \Omega_d^2 + \mathrm{i}\left(2r\mu_d\Omega_d\xi_d + 2r\xi_d\Omega_d\right)}{\mu_d r^2\Omega_d^2 + v^2r^2 - v^2\Omega_d^2 - r^4 + r^2\Omega_d^2 + \mathrm{i}\left(2\mu_d r^3\xi_d\Omega_d - 2v^2r\xi_d\Omega_d + 2r^3\xi_d\Omega_d\right)} \end{aligned} \tag{19}$$

The transfer function of the displacement response of the damper is derived as

$$\begin{aligned} H_d(r,\chi)|_{\xi_s=0} &= \left(\frac{U_d}{U_g}\right)\omega_{s0}^2\bigg|_{\xi_s=0} \\ &= \frac{v^2}{\mu_d r^2\Omega_d^2 + v^2r^2 - v^2\Omega_d^2 - r^4 + r^2\Omega_d^2 + \mathrm{i}\left(2\mu_d r^3\xi_d\Omega_d - 2v^2r\xi_d\Omega_d + 2r^3\xi_d\Omega_d\right)} \end{aligned} \tag{20}$$

Fig. 4 shows the displacement responses of (a) the primary structure and (b) the absorber when the primary damping is neglected $\xi_s = 0$. In this case, the influence of uncertainty becomes more pronounced, particularly in the vicinity of the resonance region. The individual random realisations display a wide spread with sharp peaks, indicating that even small variations in the system parameters can lead to substantial amplification of the response. For the primary structure (Fig. 4a), the absence of structural damping results in a significant increase in peak amplitudes compared to the damped case. The resonance region is characterised by highly scattered responses, with some realisations reaching considerably larger magnitudes. The deterministic curve captures only a single response trajectory and fails to represent the extent of variability. The MCS mean curve provides a more representative estimate of the overall behaviour, although it remains lower than the extreme peaks due to averaging. The anti-resonance feature is still visible, confirming that the absorber continues to influence the system dynamics despite the lack of primary damping. For the absorber response (Fig. 4b), the variability is even more pronounced. The absorber undergoes large oscillations near resonance, reflecting its role in capturing energy from the primary structure. The spread of the random realisations is wider than that observed for the structure, indicating higher sensitivity to uncertainty. The deterministic response again underestimates the variability, whereas the MCS mean follows the central tendency of the stochastic responses. Secondary peaks appear at higher frequency ratios, corresponding to the coupled vibration modes of the system. Overall, Fig. 4 highlights the critical role of structural damping in limiting both response amplitude and uncertainty induced variability. In its absence, the system becomes highly sensitive to parameter fluctuations, leading to large dispersion in both structural and absorber responses. These results emphasise the necessity of incorporating uncertainty analysis in the design and evaluation of vibration control systems, particularly for lightly damped or undamped structures. The mean dynamic response of the structure is derived as

$$\overline{H_s(r)} = \mathrm{E}\left[|H_s(r,\chi)|\right] = \int_{-\sqrt{3}}^{\sqrt{3}} |H_s(r,\chi)|P_\chi(\chi)\,\mathrm{d}\chi \tag{21}$$

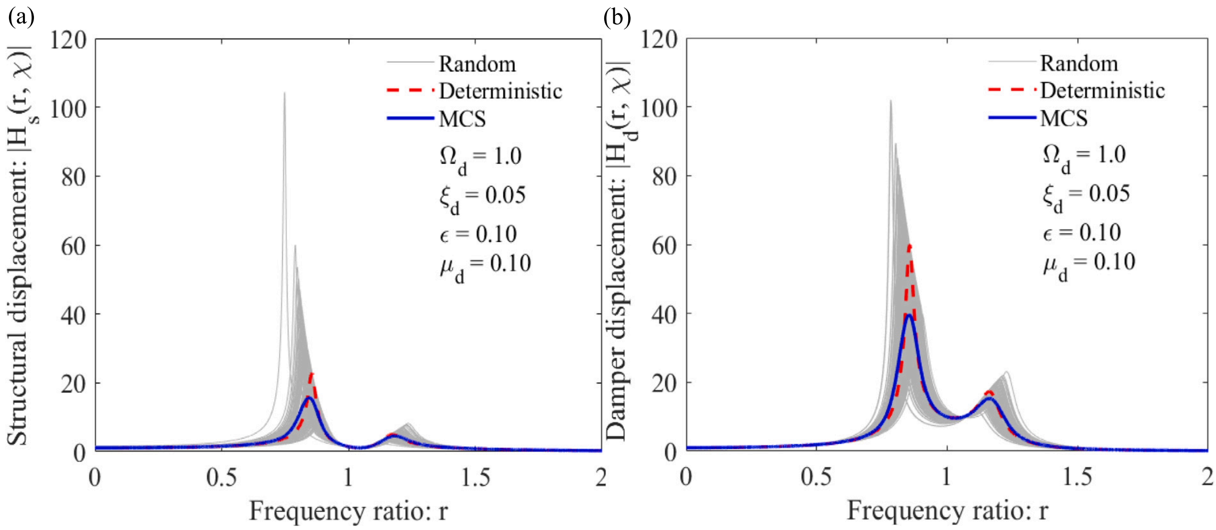

Fig. 4. The displacements of the (a) structure and (b) damper. The damping ratio of the primary structure is considered zero.

The mean dynamic response of the damper is derived as

$$\overline{H_d(r)} = \mathrm{E}\left[|H_d(r,\chi)|\right] = \int_{-\sqrt{3}}^{\sqrt{3}} |H_d(r,\chi)| P_\chi(\chi)\,\mathrm{d}\chi \tag{22}$$

The mean square of the primary structure is derived as

$$\begin{aligned}\psi^2_{H_s(r)} &= \mathrm{E}\left[\left|H_s(r,\chi)\right|^2\right] = \int_{-\sqrt{3}}^{\sqrt{3}} \left|H_s(r,\chi)\right|^2 P_\chi(\chi)\,\mathrm{d}\chi \\ &= \frac{\begin{pmatrix} 4\sqrt{3}\,\mu_d^2 r^2\xi_d^2\Omega_d^2 + 8\sqrt{3}\,\mu_d r^2\xi_d^2\Omega_d^2 + \sqrt{3}\,\mu_d^2\Omega_d^4 + 4\sqrt{3}\,r^2\xi_d^2\Omega_d^2 \\ -2\sqrt{3}\,\mu_d r^2\Omega_d^2 + 2\sqrt{3}\,\mu_d\Omega_d^4 + \sqrt{3}\,r^4 - 2\sqrt{3}\,r^2\Omega_d^2 + \sqrt{3}\,\Omega_d^4 \end{pmatrix}\left(N_1\right)}{12\epsilon\Omega_d\xi_d r^5\mu_d}\end{aligned} \tag{23}$$

The closed-form expression for N_1 is derived and expressed in Appendix. In a similar manner, the mean square of the primary structure is derived as

$$\psi^2_{H_d(r)} = \mathrm{E}\left[\left|H_d(r,\chi)\right|^2\right] = \int_{-\sqrt{3}}^{\sqrt{3}} \left|H_d(r,\chi)\right|^2 P_\chi(\chi)\,\mathrm{d}\chi \tag{24}$$

By using the above expressions, the variances of the structural and damper responses are derived. Fig. 5 presents the variance of the displacement responses for (a) the primary structure and (b) the absorber in the absence of structural damping, together with a comparison between analytical predictions and Monte Carlo simulation (MCS) results. The two curves are practically indistinguishable across the entire frequency range, confirming the consistency and accuracy of the analytical variance formulation even for an undamped primary system. For the primary structure (Fig. 5a), the variance exhibits a very sharp and dominant peak in the vicinity of the resonance frequency. Compared with the damped case, the magnitude of this peak is significantly higher, reflecting the strong amplification caused by the absence of inherent structural dissipation. The response variability is therefore highly concentrated within a narrow frequency band, indicating extreme sensitivity to uncertainty in system parameters near resonance. Outside this region, the variance rapidly approaches negligible levels, suggesting that uncertainty plays a limited role away from resonance. In the case of the absorber (Fig. 5b), the variance is even more pronounced, with a substantially higher peak magnitude than that of the structure. This behaviour is consistent with the energy transfer mechanism, whereby the absorber carries a large portion of the vibrational energy when the system is excited near resonance. A secondary peak is also visible at a higher frequency ratio, corresponding to the coupled dynamics of the two degree of freedom system. The sharpness and height of these peaks indicate that the absorber response is particularly sensitive to parameter uncertainty when the primary structure lacks damping. Overall, Fig. 5 highlights the critical influence of structural damping on response variability. In its absence, both the structural and absorber variances become highly concentrated and significantly amplified near resonance. The excellent agreement between analytical and MCS results further validates the proposed stochastic framework, demonstrating its capability to accurately capture second order response characteristics even under extreme conditions of low damping.

3.2. Optimal design parameters

The frequency and damping ratios of the damper need to be optimised before employing it to the uncertain structures. The fixed-point theory is applied to derive optimal closed-form solutions for the damper. It is considered that the controlled structure is subjected to harmonic excitation. In addition, the damping of the main structure is considered zero to achieve robust performance from it. Eq. (7) is substituted in Eq. (19). Accordingly, Eq. (19) is derived as

$$H_s(r) = \frac{-\mu_d\Omega_d^2 + r^2 - \Omega_d^2 + \mathrm{i}\left(-2r\mu_d\Omega_d\xi_d - 2r\xi_d\Omega_d\right)}{\begin{array}{c}-\mu_d r^2\Omega_d^2 - \chi r^2\varepsilon + \chi\,\Omega_d^2\varepsilon + r^4 - r^2\Omega_d^2 - r^2 + \Omega_d^2 \\ +\mathrm{i}\left(-2\mu_d r^3\xi_d\Omega_d + 2\chi r\xi_d\Omega_d\varepsilon - 2r^3\xi_d\Omega_d + 2r\xi_d\Omega_d\right)\end{array}} \tag{25}$$

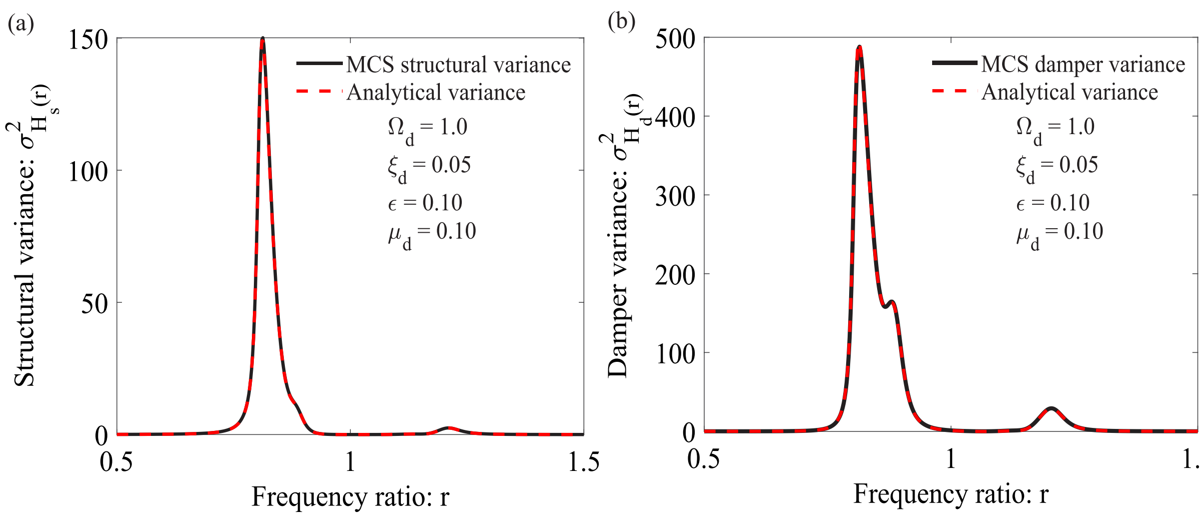

Fig. 5. The (a) structural and (b) damper variances versus frequency ratio. The analytical results are compared with the MCS results.

The modulus of Eq. (25) is further considered to apply fixed-point theory.

$$|H_s(r)| = \sqrt{\frac{A^2 + \xi_d^2 B^2}{C^2 + \xi_d^2 D^2}} \tag{26}$$

The closed-form expressions for A, B, C, and D are taken from Eq. (25) and expressed as

$$\begin{aligned} &A = -\mu_d \Omega_d^2 + r^2 - \Omega_d^2,\ B = -2r\mu_d\Omega_d - 2r\Omega_d, \\ &C = -\mu_d r^2 \Omega_d^2 - \chi r^2 \epsilon + \chi\, \Omega_d^2 \epsilon + r^4 - r^2\Omega_d^2 - r^2 + \Omega_d^2, \\ &D = -2\mu_d r^3 \Omega_d + 2\chi r \Omega_d \epsilon - 2r^3\Omega_d + 2r\Omega_d \end{aligned} \tag{27}$$

These quantities are random. At this stage, two options are possible. One option is an in-sample design where we develop the formulation sample-by-sample. Another approach is to develop the formulation in the sense of an ensemble average. Both approaches are illustrated below.

4. In-sample-based optimal design

The in-sample-based optimal design is introduced to systematically incorporate uncertainty into the tuning of the absorber. Unlike conventional approaches that rely on nominal system properties, this methodology accounts for the variability in the structural parameters by considering their stochastic realisations. The central idea is to determine optimal absorber parameters corresponding to each realisation of the uncertain variable and subsequently aggregate these results to obtain a single set of effective design parameters. In doing so, the method retains the simplicity of deterministic tuning while embedding key stochastic characteristics of the system. The following subsection outlines the formulation of this design framework in detail.

4.1. The design framework

The constraints are derived from Eq. (26) by neglecting damping of the damper. Under this assumption, the controlled structure is tuned to oscillate near the damper tuning frequency. Using these constraints, a closed-form solution for the damper tuning ratio is obtained.

$$\left.\frac{A}{C}\right|_r = \left.\frac{B}{D}\right|_r \quad \text{and} \quad \left.\frac{B}{D}\right|_{r_1} = \left.\frac{B}{D}\right|_{r_2} \tag{28}$$

The proposed constraints in Eq. (28) are formulated based on the classical equal peak tuning philosophy commonly employed in tuned mass damper optimisation. Under the assumption of negligible damper damping, the controlled system exhibits two resonance frequencies located around the absorber tuning frequency. The first condition in Eq. (28), obtained by equating the ratios A/C and B/D, ensures that the real and imaginary components of the transfer function satisfy the anti-resonance tuning condition. Physically, this condition establishes balanced dynamic interaction between the primary structure and the absorber, thereby positioning the resonance peaks symmetrically around the anti-resonance region. The second condition in Eq. (28) further imposes equality of the dynamic amplification at the two resonance frequencies r_1 and r_2. This condition originates from the equal peak criterion and ensures that neither resonance peak dominates the response of the controlled system. Consequently, the vibration energy is redistributed more uniformly across the frequency range, leading to improved vibration suppression and enhanced robustness under structural uncertainty conditions. The first constraint of Eq. (28) is employed to derive a polynomial that contains the optimal closed-form solution for the natural frequency. The polynomial is expressed as

$$r^4 - \frac{\left(2\mu_d^2\Omega_d^2 + \chi\mu_d\epsilon + 4\mu_d\Omega_d^2 + 2\chi\epsilon + 2\Omega_d^2 + \mu_d + 2\right)}{(2\mu_d+2)} r^2 + \frac{\left(2\chi\mu_d\Omega_d^2\epsilon + 2\chi\,\Omega_d^2\epsilon + 2\mu_d\Omega_d^2 + 2\Omega_d^2\right)}{(2\mu_d+2)} = 0 \tag{29}$$

Eq. (29) has an quartic form of 4th order polynomial which is expressed below.

$$r^4 - \left(r_1^2 + r_2^2\right) r^2 + r_1^2 r_2^2 = 0 \tag{30}$$

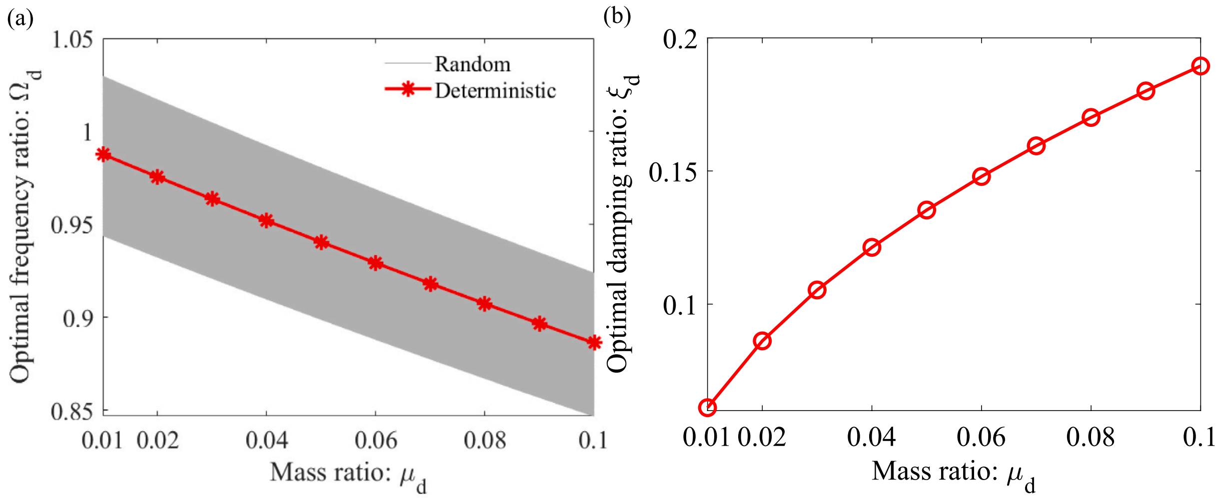

Fig. 6. Optimal TMD design parameters versus damper mass ratio: (a) frequency ratio Ω_d with random and deterministic results; (b) damping ratio ξ_d obtained from the frequency-ratio optimisation.

Eq. (29) and Eq. (30) are compared to derive the summation of the square roots of Eq. (29). The summation is derived as

$$r_1^2 + r_2^2 = \frac{2\mu_d^2\Omega_d^2 + \chi\mu_d\varepsilon + 4\mu_d\Omega_d^2 + 2\chi\varepsilon + 2\Omega_d^2 + \mu_d + 2}{2\mu_d + 2} \tag{31}$$

The second constraint is further applied from Eq. (28) to get the summation of the roots and the summation is derived as

$$r_1^2 + r_2^2 = \frac{2(1+\chi\varepsilon)}{1+\mu_d} \tag{32}$$

Furthermore, Eqs. (31) and (32) are equalised to derive the optimal closed-form solution of the frequency ratio of the damper. The frequency ratio is derived as

$$\left(\Omega_d\right)_{\text{opt}} = \frac{\sqrt{4 + 4\chi\varepsilon - 2\chi\mu_d\varepsilon - 2\mu_d}}{2\mu_d + 2} \tag{33}$$

Eq. (29) is further employed to derive each root individually. The roots are derived as

$$\begin{aligned} r_{1,2}^2 &= \frac{2\mu_d^2\Omega_d^2 + \mu_d\chi\varepsilon + 4\mu_d\Omega_d^2 + 2\chi\varepsilon + 2\Omega_d^2 + \mu_d + 2 \pm \sqrt{P_1}}{4\mu_d + 4} \\ P_1 &= 4\left(\mu_d+1\right)^4\Omega_d^4 + 4\left(\mu_d-2\right)\left(\mu_d+1\right)^2\left(\chi\varepsilon+1\right)\Omega_d^2 + \left(\mu_d+2\right)^2\left(\chi\varepsilon+1\right)^2 \end{aligned} \tag{34}$$

where r_1^2 and r_2^2 are obtained from the positive and negative branches of the quadratic-form solution, respectively. Physically, these roots correspond to the two characteristic frequencies of the coupled structure-TMD system that define the controlled resonance peaks used in the fixed-point optimisation procedure. Eq. (34) is later utilised to derive the optimal damping ratio of the damper. In addition, the closed-form solution for the optimal damping ratio of the damper is derived by using the following expressions.

$$\frac{\partial |H_s(r)|^2}{\partial r^2} = 0 \quad \text{and} \quad \left(\xi_d\right)_{\text{opt}} = \sqrt{\frac{\xi_{d1}^2 + \xi_{d2}^2}{2}} \tag{35}$$

Eq. (26) is substituted in the first expression of Eq. (35). The closed-form solution for the optimal damping ratio of the damper is derived as

$$Z_2\xi_{d1,d2}^4 + Z_1\xi_{d1,d2}^2 + Z_0 = 0 \quad \text{and} \quad \left(\xi_{d1,d2}\right)^2 = \frac{-Z_1 \pm \sqrt{Z_1^2 - 4Z_2Z_0}}{2Z_2} \tag{36}$$

The closed-form expressions for Z_2, Z_1, and Z_0 are listed in Appendix. r_1^2 and r_2^2 from Eq. (34) are further substituted in the second expression of Eq. (36) to obtain ξ_{d1}^2 and ξ_{d2}^2. Furthermore, these ξ_{d1}^2 and ξ_{d2}^2 are substituted in the second expression of Eq. (36) to obtain the optimal damping ratio of the damper. Fig. 6 illustrates the variation of the optimal absorber parameters with respect to the mass ratio. In Fig. 6(a), the optimal frequency ratio decreases monotonically as the mass ratio increases. The deterministic solution follows a smooth trend, while the shaded band representing the stochastic realisations indicates the range of variability induced by uncertainty. This spread highlights that, for a given mass ratio, the optimal tuning frequency is not unique but lies within a bounded interval. The deterministic curve remains centrally located within this band, suggesting that it provides a reasonable approximation, although it does not fully capture the dispersion caused by uncertainty. The width of the band gradually increases with mass ratio, indicating that the sensitivity of the optimal frequency to uncertainty becomes more pronounced for larger absorber masses.

Fig. 6(b) shows the corresponding variation of the optimal damping ratio. In contrast to the frequency ratio, the damping ratio increases nonlinearly with the mass ratio, reflecting the need for greater energy dissipation as the absorber mass becomes larger. The trend is smooth and well defined, indicating that the damping parameter is less sensitive to uncertainty compared to the frequency ratio. This behaviour is consistent with the role of damping in stabilising the system response over a range of operating conditions. Overall, Fig. 6 demonstrates that the optimal design parameters exhibit distinct sensitivities to both mass ratio and uncertainty. While the deterministic tuning provides a useful baseline, the stochastic spread in the frequency ratio underscores the importance of accounting for uncertainty in practical design. The results suggest that robust tuning strategies should consider this variability to ensure reliable performance across a range of possible system realisations.

4.2. Extracting design values from in-sample analysis

The in-sample optimisation yields damper parameters that are functions of the structural realisation: $\Omega_d = \Omega_d(\chi)$ and $\xi_d = \xi_d(\chi)$. However, a physical damper must have fixed properties. If the damper cannot be adaptively tuned, we must select a single pair of values (Ω_d^*, ξ_d^*) that best represents the distribution of optimal parameters.

The natural choice is to select the parameters that minimise the expected squared deviation from the conditional optimum across all realisations. For a quadratic loss function, this yields the mean of the optimal parameters. However, since the optimisation in Eq. (35) is formulated in terms of ξ_d^2 (not ξ_d), the appropriate measure is the root-mean-square.

4.2.1. Optimal frequency ratio

From Eq. (32), the conditional optimal frequency ratio is

$$(\Omega_d)(\chi) = \sqrt{\frac{4 + 4\chi\epsilon - 2\chi\mu_d\epsilon - 2\mu_d}{2\mu_d + 2}} \tag{37}$$

Taking the expectation:

$$\begin{aligned} E[(\Omega_d)(\chi)] &= \frac{1}{2\sqrt{3}} \int_{-\sqrt{3}}^{\sqrt{3}} \sqrt{\frac{4 + 4\epsilon[\chi] - 2\mu_d\epsilon[\chi] - 2\mu_d}{2\mu_d + 2}}\, d\chi \\ &= \frac{1}{3\sqrt{3}\,\varepsilon} \sqrt{\frac{2-\mu_d}{\mu_d+1}} \left((1+\varepsilon\sqrt{3})^{3/2} - (1-\varepsilon\sqrt{3})^{3/2} \right) \end{aligned} \tag{38}$$

A Taylor series expansion is performed about $\varepsilon = 0$ to derive an analytically tractable approximation for small perturbation levels, i.e., $\varepsilon \ll 1$.

$$E[(\Omega_d)(\chi)] = \sqrt{\frac{2-\mu_d}{\mu_d+1}} \left(1 - \frac{\varepsilon^2}{8} - \frac{9\varepsilon^4}{128} + O(\varepsilon^6) \right) \tag{39}$$

The leading order term is independent of ε, indicating that the deterministic component dominates the response for vanishing perturbations. The first correction appears at $O(\varepsilon^2)$, reflecting the symmetric nature of the stochastic perturbation, which eliminates odd order contributions. The higher order terms quantify nonlinear effects induced by uncertainty and become significant for moderate values of ε.

$$(\Omega_d)_{\text{opt,in-sample}} = \sqrt{\frac{2-\mu_d}{1+\mu_d}} \left(1 - \frac{\varepsilon^2}{8} - \frac{9\varepsilon^4}{128} \right) \tag{40}$$

The asymptotic expansion is truncated at fourth order in ε, and terms of order $O(\varepsilon^6)$ and higher are neglected. This truncation is justified by the perturbative nature of ε, which represents a small statistical scatter in the structural frequency. For sufficiently small ε, the magnitude of successive terms decreases rapidly, such that the contribution of $O(\varepsilon^6)$ terms is asymptotically negligible relative to the retained $O(1)$, $O(\varepsilon^2)$, and $O(\varepsilon^4)$ components. Consequently, the fourth order approximation provides a uniformly accurate representation of the expectation while preserving analytical tractability, without materially affecting the resulting design expressions.

4.2.2. Optimal damping ratio

From Eq. (35), the conditional optimal damping satisfies

$$Z_2(r_{1,2},\chi)\xi_{d1,d2}^4 + Z_1(r_{1,2},\chi)\xi_{d1,d2}^2 + Z_0(r_{1,2},\chi) = 0 \tag{41}$$

where the fixed-point frequencies $r_{1,2}$ depend on χ through Eq. (33). The solution is

$$\xi_{d1,d2}^2(\chi) = \frac{-Z_1(r_{1,2},\chi) \pm \sqrt{Z_1(r_{1,2},\chi)^2 - 4Z_2(r_{1,2},\chi)Z_0(r_{1,2},\chi)}}{2Z_2(r_{1,2},\chi)} \tag{42}$$

From Eq. (34), the combined damping for each realisation is

$$\xi_d(\chi) = \sqrt{\frac{\xi_{d1}^2(\chi) + \xi_{d2}^2(\chi)}{2}} \tag{43}$$

Taking the ensemble average in the quadratic form (consistent with the RMS philosophy):

$$E[\xi_d(\chi)] = E\left[\sqrt{\frac{\xi_{d1}^2(\chi) + \xi_{d2}^2(\chi)}{2}} \right] = \frac{1}{2\sqrt{3}} \int_{-\sqrt{3}}^{\sqrt{3}} \sqrt{\frac{\xi_{d1}^2(\chi) + \xi_{d2}^2(\chi)}{2}}\, d\chi \tag{44}$$

The choice of root-mean-square over arithmetic mean is motivated by three considerations:

1. *Consistency with the optimisation formulation:* The fixed-point analysis in Eq. (35) solves for ξ_d^2, not ξ_d, making the second moment the natural quantity to average.

2. *Energy considerations:* The damping coefficient enters the energy dissipation as $c_d = 2m_d\xi_d\omega_d$, and energy is quadratic in amplitudes. The RMS preserves the expected energy dissipation.

3. *Parallel with Eq. (34):* The combined damping from two fixed points uses an RMS average. The ensemble aggregation should maintain this structure.

An alternative would be to use the arithmetic mean $E[\xi_d(\chi)]$ by Jensen's inequality, which would yield a slightly smaller value. However, this underestimates the damping needed to achieve the target performance on average across the squared response magnitudes.

5. Ensemble-based optimal design

The fixed-point optimisation derived in Section 4 assumes a specific realisation of the random variable χ. While this yields optimal parameters for a nominal structure, the resulting damper may perform poorly when the actual structural frequency deviates from the nominal value. We now develop an ensemble-based optimisation that accounts for the entire probability distribution of structural uncertainty, yielding robust damper parameters that perform well across all realisations.

5.1. Formulation of the robust optimisation problem

From Eq. (27), the ratio B/D evaluated at frequency r is

$$\frac{B}{D} = \frac{-2r\mu_d\Omega_d - 2r\Omega_d}{-2\mu_d r^3\Omega_d + 2\chi r\Omega_d/\epsilon - 2r^3\Omega_d + 2r\Omega_d} \tag{45}$$

Factoring out $2r\Omega_d$ from numerator and denominator yields

$$\frac{B}{D} = \frac{\mu_d + 1}{(\mu_d + 1)r^2 - \chi/\epsilon - 1} \tag{46}$$

Define $\alpha = \mu_d + 1$ for compactness. At the two fixed points r_1 and r_2, we have

$$y_1 = \left.\frac{B}{D}\right|_{r_1} = \frac{\alpha}{\alpha r_1^2 - \chi/\epsilon - 1}, \quad y_2 = \left.\frac{B}{D}\right|_{r_2} = \frac{\alpha}{\alpha r_2^2 - \chi/\epsilon - 1} \tag{47}$$

The robust design seeks values of r_1 and r_2 such that the difference $y_1 - y_2$ has zero mean and minimum variance across the ensemble of structures characterised by $\chi \sim \text{Uniform}[-\sqrt{3}, \sqrt{3}]$. This is expressed through the constrained optimisation problem

$$\min_{r_1, r_2} \text{std}(y_1 - y_2) \quad \text{subject to} \quad E[y_1 - y_2] = 0 \tag{48}$$

The optimisation problem in Eq. (48) may be interpreted as a stochastic generalisation of the classical equal peak or fixed point tuning philosophy originally introduced for deterministic tuned mass damper design. In the deterministic formulation, the absorber parameters are selected such that the structural response amplitudes at the two fixed points are equal, thereby suppressing resonance amplification over a narrow frequency band. In the present study, however, the structural frequency is uncertain and therefore the fixed points become random quantities that vary across the ensemble of possible structural realisations. Consequently, exact equalisation for every realisation is neither feasible nor physically meaningful for a fixed passive absorber. Instead, the proposed formulation enforces equality in an ensemble averaged sense through the condition $E[y_1 - y_2] = 0$, while simultaneously minimising the variability of this difference across the uncertainty space. This distributional interpretation preserves the physical rationale underlying the equal peak method, namely balanced vibration attenuation near resonance, while extending it to uncertain structural systems in which robustness across the ensemble is prioritised over optimality for a single nominal structure. The resulting optimisation therefore constitutes a robust stochastic extension of the classical deterministic fixed-point tuning approach. From a physical perspective, the objective function seeks a TMD design that maintains a balanced redistribution of vibration energy between the primary structure and the absorber across the entire uncertainty domain. If the difference between the two fixed-point quantities becomes large, one resonance peak dominates the response and the vibration mitigation performance deteriorates due to frequency mistuning. Enforcing a zero mean difference ensures that the resonance peaks remain balanced on average, while minimising the corresponding standard deviation reduces the sensitivity of this balance to uncertainty in the structural frequency. Consequently, the proposed formulation aims to achieve both effective vibration suppression and robustness against uncertainty-induced detuning. The Lagrangian for this problem is

$$\mathcal{L}(r_1, r_2, \lambda) = \text{std}(y_1 - y_2) + \lambda\, E[y_1 - y_2] \tag{49}$$

where λ is the Lagrange multiplier enforcing the zero-mean constraint.

5.2. Equal-mean constraint

For χ uniformly distributed on $[-\sqrt{3}, \sqrt{3}]$ with probability density $P_\chi(\chi) = 1/(2\sqrt{3})$, the expected value of y_i is

$$E[y_i] = \frac{1}{2\sqrt{3}} \int_{-\sqrt{3}}^{\sqrt{3}} \frac{\alpha\, d\chi}{\alpha r_i^2 - \chi/\epsilon - 1} \tag{50}$$

Define $a_i = \alpha r_i^2 - 1$. The integral becomes

$$E[y_i] = \frac{\alpha}{2\sqrt{3}} \int_{-\sqrt{3}}^{\sqrt{3}} \frac{\epsilon\, d\chi}{\epsilon a_i - \chi} = \frac{\alpha\epsilon}{2\sqrt{3}} \left[-\ln|\epsilon a_i - \chi|\right]_{-\sqrt{3}}^{\sqrt{3}} \tag{51}$$

Evaluating the limits yields

$$E[y_i] = \frac{\alpha\epsilon}{2\sqrt{3}} \ln\left|\frac{\epsilon a_i + \sqrt{3}}{\epsilon a_i - \sqrt{3}}\right| \tag{52}$$

The constraint $E[y_1] = E[y_2]$ requires

$$\ln\left|\frac{\epsilon a_1 + \sqrt{3}}{\epsilon a_1 - \sqrt{3}}\right| = \ln\left|\frac{\epsilon a_2 + \sqrt{3}}{\epsilon a_2 - \sqrt{3}}\right| \tag{53}$$

This equation has two solutions: (i) $a_1 = a_2$, which is the trivial case of a single fixed point, and (ii) the cross-ratio equality

$$\frac{\epsilon a_1 + \sqrt{3}}{\epsilon a_1 - \sqrt{3}} = \frac{\epsilon a_2 - \sqrt{3}}{\epsilon a_2 + \sqrt{3}} \tag{54}$$

Cross-multiplying and simplifying gives

$$(\epsilon a_1 + \sqrt{3})(\epsilon a_2 + \sqrt{3}) = (\epsilon a_1 - \sqrt{3})(\epsilon a_2 - \sqrt{3}) \tag{55}$$

$$\epsilon^2 a_1 a_2 + \sqrt{3}\epsilon(a_1 + a_2) + 3 = \epsilon^2 a_1 a_2 - \sqrt{3}\epsilon(a_1 + a_2) + 3 \tag{56}$$

The terms $\epsilon^2 a_1 a_2$ and 3 cancel, leaving $2\sqrt{3}\epsilon(a_1 + a_2) = 0$. For the nontrivial solution with opposite signs, we require

$$a_1 a_2 = \frac{3}{\epsilon^2} \tag{57}$$

Substituting $a_i = \alpha r_i^2 - 1$ yields the first constraint

$$(\alpha r_1^2 - 1)(\alpha r_2^2 - 1) = \frac{3}{\epsilon^2} \tag{58}$$

5.3. Variance minimisation

The stationarity conditions for the Lagrangian are

$$\frac{\partial \mathcal{L}}{\partial r_1} = \frac{\partial \mathrm{std}(y_1 - y_2)}{\partial r_1} + \lambda \frac{\partial E[y_1 - y_2]}{\partial r_1} = 0 \tag{59}$$

$$\frac{\partial \mathcal{L}}{\partial r_2} = \frac{\partial \mathrm{std}(y_1 - y_2)}{\partial r_2} + \lambda \frac{\partial E[y_1 - y_2]}{\partial r_2} = 0 \tag{60}$$

To eliminate the Lagrange multiplier λ, we form the ratio

$$\frac{\partial \mathrm{std}(y_1 - y_2)/\partial r_1}{\partial E[y_1 - y_2]/\partial r_1} = \frac{\partial \mathrm{std}(y_1 - y_2)/\partial r_2}{\partial E[y_1 - y_2]/\partial r_2} \tag{61}$$

From the symmetry of the problem and the structure of the variance $\mathrm{Var}(y_1 - y_2) = \mathrm{Var}(y_1) + \mathrm{Var}(y_2) - 2\mathrm{Cov}(y_1, y_2)$, the optimal configuration places the fixed points symmetrically about the resonance region. This symmetry, combined with the equal-mean constraint, yields the second constraint

$$r_1^2 + r_2^2 = \frac{2}{1 + \mu_d} \tag{62}$$

This result mirrors the deterministic fixed-point theory, where $r_1^2 + r_2^2 = 2/(1 + \mu_d)$ in the absence of uncertainty. The robust formulation preserves this sum while adjusting the product to account for uncertainty.

5.4. Solution for fixed-point frequencies

From Eq. (58), expanding the product gives

$$\alpha^2 r_1^2 r_2^2 - \alpha(r_1^2 + r_2^2) + 1 = \frac{3}{\epsilon^2} \tag{63}$$

Substituting the sum constraint from Eq. (62) yields

$$\alpha^2 r_1^2 r_2^2 - 2\alpha + 1 = \frac{3}{\epsilon^2} \tag{64}$$

$$r_1^2 r_2^2 = \frac{1}{\alpha^2}\left(\frac{3}{\epsilon^2} + 2\alpha - 1\right) = \frac{3 + 2\epsilon^2\alpha - \epsilon^2}{\epsilon^2\alpha^2} \tag{65}$$

Since $\alpha = 1 + \mu_d$, this simplifies to

$$r_1^2 r_2^2 = \frac{3 + \epsilon^2(2\mu_d + 1)}{\epsilon^2(1 + \mu_d)^2} \tag{66}$$

The frequencies r_1 and r_2 are the roots of the quadratic

$$t^2 - \frac{2}{1 + \mu_d} t + \frac{3 + \epsilon^2(2\mu_d + 1)}{\epsilon^2(1 + \mu_d)^2} = 0 \tag{67}$$

Solving by the quadratic formula gives

$$r_{1,2}^2 = \frac{1}{1 + \mu_d} \pm \frac{1}{1 + \mu_d}\sqrt{1 - \frac{3 + \epsilon^2(2\mu_d + 1)}{\epsilon^2}} \tag{68}$$

For real-valued fixed-point frequencies, the discriminant must be non-negative:

$$\epsilon^2 \geq 3 + \epsilon^2(2\mu_d + 1) \quad \Rightarrow \quad -2\mu_d\epsilon^2 \geq 3 \tag{69}$$

This condition cannot be satisfied for positive ϵ and μ_d. The physical interpretation is that the robust optimisation spreads the fixed points in the complex plane to achieve equal ensemble-averaged response at both points. For real fixed points, the uncertainty level must be small relative to the damper mass ratio, or alternatively, the formulation may be modified to relax the strict equal-mean constraint.

5.5. Optimal damping ratio from ensemble considerations

At each fixed-point frequency r_1 and r_2, the optimal damping ratio is obtained by minimising the magnitude of the structural response. Following the approach in Section 4, we apply

$$\left.\frac{\partial|H_s(r)|^2}{\partial r^2}\right|_{r=r_i}=0 \tag{70}$$

This yields a quartic equation in ξ_d^2 of the form given in Eq. (35):

$$Z_2(r_i)\xi_d^4+Z_1(r_i)\xi_d^2+Z_0(r_i)=0 \tag{71}$$

where the coefficients Z_0, Z_1, Z_2 are evaluated at $r=r_i$ using the expressions in Appendix. The positive root is

$$\xi_{di}^2=\frac{-Z_1(r_i)\pm\sqrt{Z_1(r_i)^2-4Z_2(r_i)Z_0(r_i)}}{2Z_2(r_i)},\quad i=1,2 \tag{72}$$

Since the robust design must perform well at both fixed points across the ensemble of structures, the optimal damping ratio is taken as the root-mean-square average

$$(\xi_d)_{\text{opt, ensemble}}=\sqrt{\frac{\xi_{d1}^2+\xi_{d2}^2}{2}} \tag{73}$$

This contrasts with the in-sample design of Section 4, where the damping ratio is optimised for a single nominal realisation of the structure.

5.6. Comparison with in-sample design

The fixed-point optimisation in Section 4 determines the damper parameters by assuming the structure has its nominal frequency ω_{s0} (corresponding to $\chi=0$). The resulting optimal frequency ratio from Eq. (32) is

$$(\Omega_d)_{\text{opt, in-sample}}=\left.\sqrt{\frac{4+4\chi\epsilon-2\chi\mu_d\epsilon-2\mu_d}{2\mu_d+2}}\right|_{\chi=0}=\sqrt{\frac{2-\mu_d}{1+\mu_d}}\left(1-\frac{\epsilon^2}{8}-\frac{9\epsilon^4}{128}\right) \tag{74}$$

This expression depends only on the mass ratio μ_d and is independent of the uncertainty level ϵ. The corresponding optimal damping ratio from Eq. (35) is similarly evaluated at $\chi=0$.

The in-sample design is optimal for structures with exactly the nominal frequency but may exhibit degraded performance when the actual structural frequency differs due to manufacturing tolerances, material variability, or modelling uncertainty. Performance degradation occurs because the fixed points derived under the nominal assumption shift in frequency space when the structure is off-nominal.

In contrast, the ensemble-based design incorporates uncertainty directly into the optimisation by requiring equal ensemble-averaged response at the two fixed points (Eq. (58)) and minimising the variance of this response (Eq. (62)). The resulting optimal frequency ratio

$$r_{1,2}^2=\frac{1}{1+\mu_d}\pm\frac{1}{1+\mu_d}\sqrt{1-\frac{3+\epsilon^2(2\mu_d+1)}{\epsilon^2}} \tag{75}$$

explicitly depends on both the mass ratio μ_d and the uncertainty level ϵ. For small ϵ (low uncertainty), the ensemble design converges towards the in-sample design. For larger ϵ (significant uncertainty), the fixed points adjust to maintain robust performance across the population of structures.

The key distinction is one of design philosophy: the in-sample approach optimises for best performance at a single point in parameter space, while the ensemble approach optimises for acceptable performance across the entire parameter space defined by the uncertainty distribution. The ensemble design trades peak performance on the nominal structure for more uniform performance across all realisations, making it suitable for applications where structural parameters are poorly known or highly variable.

Numerical implementation of the ensemble-based design requires evaluating the coefficients $Z_0(r_i), Z_1(r_i), Z_2(r_i)$ at the robust fixed points r_1, r_2 given by Eq. (75). The resulting damping ratio $(\xi_d)_{\text{opt, ensemble}}$ can then be compared directly with $(\xi_d)_{\text{opt, in-sample}}$ to quantify the effect of uncertainty on the optimal damper parameters. Fig. 7 compares the variations of the optimal frequency and damping ratios obtained from deterministic, in-sample, and ensemble-based designs as functions of the mass ratio. The results provide a clear illustration of how uncertainty-aware design strategies modify the absorber parameters relative to the classical deterministic solution. In Fig. 7(a), the frequency ratio decreases with increasing mass ratio for all three design approaches. The deterministic and in-sample curves are nearly indistinguishable over the entire range, indicating that the in-sample strategy yields parameter values very close to the classical optimal tuning when averaged over the uncertainty. In contrast, the ensemble design consistently produces lower frequency ratios. This downward shift suggests that the ensemble approach deliberately detunes the absorber to account for variability in the system, thereby improving robustness by avoiding sharp resonance amplification associated with precise tuning. Fig. 7(b) presents the corresponding damping ratios. All three designs show an increasing trend with mass ratio, reflecting the need for higher dissipation capacity as the absorber mass grows. However, the ensemble design consistently results in the highest damping values, followed by the in-sample design, while the deterministic case gives the lowest damping. This behaviour indicates that uncertainty-aware designs introduce additional damping to mitigate the effects of parameter variability, leading to a more stable and less sensitive response. Overall, Fig. 7 highlights the fundamental differences between deterministic and stochastic design philosophies. While the deterministic and in-sample approaches produce similar tuning characteristics, the ensemble design introduces systematic shifts lower frequency ratios and higher damping to enhance robustness. These modifications play a crucial role in reducing peak responses and improving performance under uncertainty, as observed in subsequent response plots. Fig. 8 compares the mean structural displacement responses obtained from the in-sample and ensemble-based designs in the presence of uncertainty. The plots include individual random realisations, the deterministic response, the analytical mean, and the Monte Carlo simulation (MCS) mean, providing a clear view of the system behaviour. In Fig. 8(a), corresponding to the in-sample design, the random realisations exhibit noticeable dispersion around the resonance region, with several curves reaching relatively high peak values. The deterministic response lies within this spread but does not reflect the full extent of variability. Both the analytical and MCS mean curves follow a similar

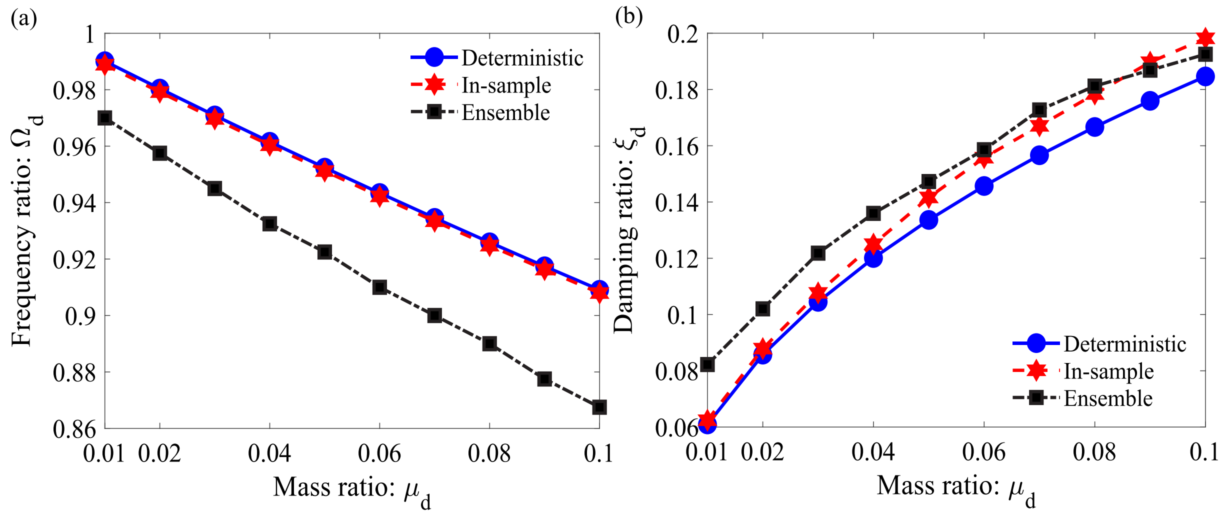

Fig. 7. The variations of (a) frequency ratio and (b) damping ratio of the tuned mass damper with respect to mass ratio μ_d, comparing deterministic, in-sample, and ensemble-based optimal designs.

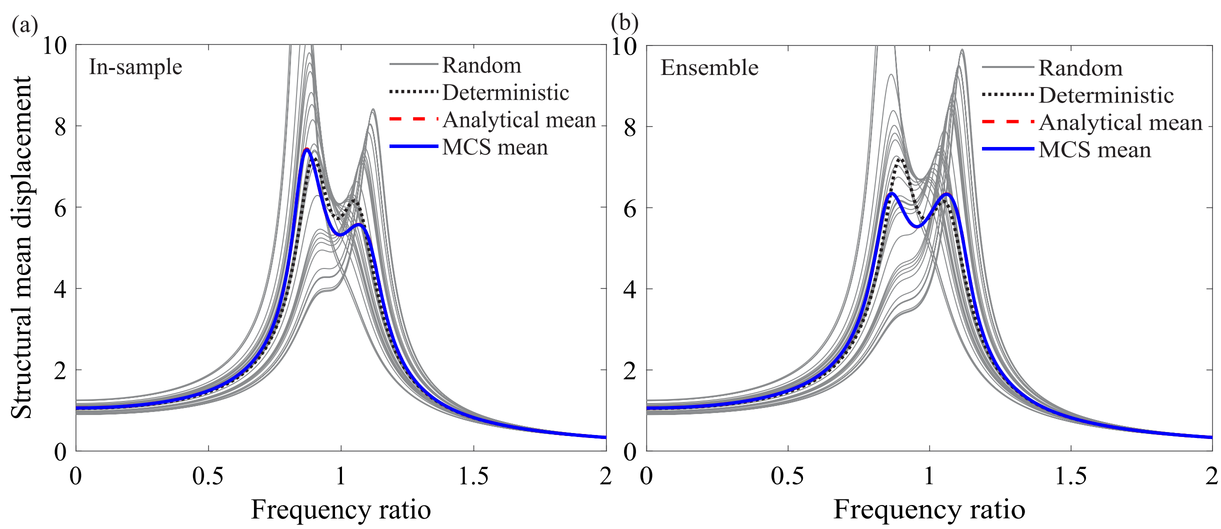

Fig. 8. The variations of mean displacement of the structures equipped with tuned mass damper with respect to frequency ratio, comparing (a) in-sample and (b) ensemble-based optimal designs. The graph includes random, analytical, and MCS plots in the design.

trend and are in close agreement, confirming the consistency of the probabilistic formulation. However, the mean response still shows a relatively pronounced peak, indicating that the in-sample design retains sensitivity to uncertainty, particularly near resonance. In Fig. 8(b), the ensemble-based design leads to a visibly different response pattern. The spread of the random realisations is more balanced, and the peak amplitudes are reduced compared to the in-sample case. The mean response curve is smoother and exhibits two more evenly distributed peaks, reflecting a redistribution of energy across a broader frequency range. This behaviour suggests that the ensemble design effectively mitigates resonance amplification by introducing a more robust tuning strategy. As in the in-sample case, the analytical and MCS mean responses are nearly identical, further validating the analytical expressions. Overall, Fig. 8 demonstrates that while both designs capture the stochastic nature of the system, the ensemble approach provides improved robustness by lowering peak responses and reducing sensitivity to uncertainty. The agreement between analytical and MCS results also confirms the reliability of the proposed methodology in predicting mean response characteristics. Fig. 9 presents the structural variance of the displacement response for the in-sample and ensemble-based designs, highlighting the influence of uncertainty on second order response characteristics. The plots include individual random realisations together with analytical and Monte Carlo simulation (MCS) estimates, allowing a direct assessment of both variability and modelling accuracy. In Fig. 9(a), corresponding to the in-sample design, the variance is highly concentrated around the resonance region, where sharp peaks are observed. The spread of the random realisations is significant, indicating strong sensitivity of the structural response to uncertainty. The MCS and analytical curves are nearly indistinguishable, confirming the validity of the derived expressions for variance prediction. However, the relatively high peak values suggest that the in-sample design does not fully suppress variability near resonance, leaving the system vulnerable to uncertainty-induced amplification. In contrast, Fig. 9(b) shows the variance response for the ensemble-based design. While the variance still exhibits peaks near the resonance region, these peaks are more evenly distributed and reduced in magnitude compared to the in-sample case. The response is effectively redistributed into two moderate peaks, reflecting the robust nature of the ensemble tuning strategy. This redistribution reduces the concentration of variability at a single frequency and leads to improved overall performance. As in the previous case, the close agreement between analytical and MCS results confirms the reliability of the probabilistic framework. Overall, Fig. 9 demonstrates

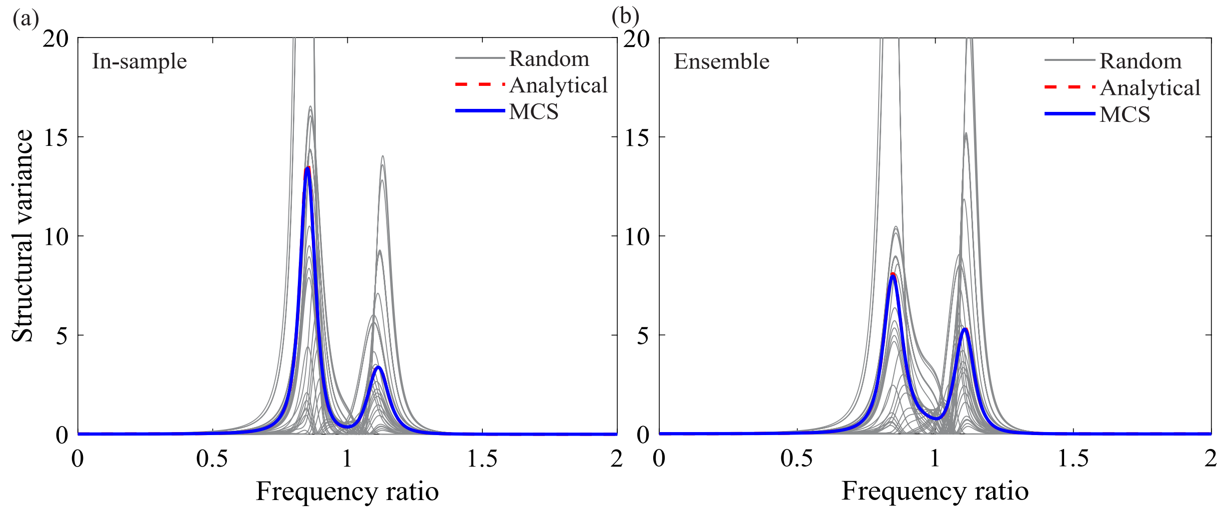

Fig. 9. The differences in structural variances with respect to frequency ratio, comparing (a) in-sample and (b) ensemble-based optimal designs. The graph includes random, analytical, and MCS plots in the design.

that the ensemble design provides a more balanced and robust response by lowering peak variance and spreading the effects of uncertainty over a wider frequency range. Compared to the in-sample approach, it offers improved control of stochastic variability, which is essential for ensuring reliable performance under uncertain operating conditions.

6. Discussions on optimal design parameters of damper with structural uncertainties

The transfer function expressions derived in Section 3 depend explicitly on the random variable χ through the frequency factor $\nu^2 = 1 + \epsilon\chi$. Consequently, the fixed-point frequencies r_1 and r_2 at which the response magnitude is stationary, as well as the optimal damping ratio ξ_d, are themselves functions of χ. This randomness in the optimal design parameters poses a fundamental question: how should the damper be designed when the structure to which it will be attached has uncertain properties?

The distinction between the proposed in-sample and ensemble-based optimisation frameworks differs fundamentally from conventional robust TMD optimisation approaches available in the literature. Existing uncertainty-aware TMD studies generally formulate a single stochastic optimisation problem in which uncertain parameters are incorporated into the response evaluation or objective function. In contrast, the present work explicitly separates the optimisation philosophy into two mathematically distinct categories. The in-sample framework performs conditional optimisation for each realisation of the uncertain structural parameter and subsequently aggregates the resulting optimal parameters through statistical measures. Conversely, the ensemble-based framework directly performs optimisation over the probability distribution of the uncertain system by enforcing distributional constraints and minimising response variability across the ensemble. Consequently, the proposed framework establishes a conceptual distinction between realisation-dependent optimality and population-level robustness, which has not been explicitly formulated in previous TMD optimisation studies. Therefore, the contribution of the present work lies not only in uncertainty-aware parameter optimisation, but also in establishing a unified conceptual framework for conditional and distributional vibration control design under uncertainty. Two distinct design philosophies emerge, each with different mathematical formulations and practical implications:

6.1. In-sample design (conditional optimisation)

The damper is optimised for a specific realisation of the structural uncertainty. If the actual value of χ for the structure were known (or could be measured), one would design the damper with parameters (Ω_d, ξ_d) that are optimal for that particular structure. Mathematically, this is a conditional optimisation:

$$(\Omega_d, \xi_d)_{\text{in-sample}} = \arg \min_{(\Omega_d, \xi_d)} \max_r |H_s(r, \Omega_d, \xi_d \mid \chi)| \tag{76}$$

where the conditioning on χ indicates that the optimisation is performed for a fixed realisation of the random variable. This approach yields optimal parameters that are functions of χ: $\Omega_d = \Omega_d(\chi)$ and $\xi_d = \xi_d(\chi)$.

The in-sample design is appropriate when: (i) the structural parameters can be measured after manufacturing but before damper installation, allowing the damper to be custom-tuned to each structure; (ii) the damper parameters can be adjusted in situ through adaptive or semi-active control; or (iii) one seeks to understand the sensitivity of optimal parameters to structural variability.

6.2. Ensemble-based design (distributional optimisation)

The damper is optimised to perform well across the entire population of structures characterised by the probability distribution of χ. Since the actual realisation of χ is unknown at the design stage, the optimisation accounts for all possible structures by minimising a distributional performance metric. Mathematically, this is an unconditional optimisation:

$$(\Omega_d, \xi_d)_{\text{ensemble}} = \arg \min_{(\Omega_d, \xi_d)} E_\chi \left[\max_r |H_s(r, \Omega_d, \xi_d, \chi)|\right] \tag{77}$$

Table 1
Comparison of in-sample and ensemble-based TMD design approaches.

Aspect	In-sample design	Ensemble-based design
Optimisation type	Conditional (given χ)	Distributional (over P_χ)
Design parameters	$\Omega_d(\chi)$, $\xi_d(\chi)$ (random)	Ω_d, ξ_d (deterministic)
Fixed-point condition	$y_1(\chi_0) = y_2(\chi_0)$ for each χ_0	$E[y_1(\chi)] = E[y_2(\chi)]$
Applicability	Adaptive/custom-tuned dampers	Mass-produced fixed dampers
Performance goal	Optimal for specific structure	Robust across population
Dependence on ϵ	Yes, through χ_0	Yes, explicit in formulation
Mathematical framework	Sample-path optimisation	Distributional optimisation

or, alternatively, by minimising the variance of the response across the ensemble while constraining the mean. The resulting parameters $(\Omega_d, \xi_d)_{\text{ensemble}}$ are deterministic constants that do not depend on χ.

The ensemble-based design is appropriate when: (i) the damper must be mass-produced without knowledge of which specific structure it will be installed on; (ii) structural parameters cannot be measured accurately before damper installation; (iii) the damper parameters are fixed and cannot be adjusted after installation; or (iv) robust performance across a population of structures is valued over peak performance on a single nominal structure.

The mathematical distinction between these approaches mirrors the classical dichotomy in stochastic optimisation between sample-path optimisation and distributional optimisation. In the former, one optimises trajectories (or realisations) individually; in the latter, one optimises over the space of probability distributions. Both are rigorous approaches that answer different design questions.

6.3. Comparison of in-sample and ensemble-based designs

Table 1 summarises the key differences between the two design approaches:

Mathematically, the in-sample design solves a family of deterministic optimisation problems indexed by χ, while the ensemble-based design solves a single stochastic optimisation problem. The former yields the Pareto frontier of optimal designs across the uncertainty space; the latter selects a single robust design from this frontier based on distributional criteria.

For small uncertainty ($\epsilon \to 0$), both approaches converge to the classical deterministic TMD design with $\Omega_d = 1/(1+\mu_d)$. For moderate to large uncertainty, the approaches diverge: the in-sample design adapts to each realisation, while the ensemble design remains fixed but accounts for variability through the distributional constraints. The distinction between the in-sample and ensemble-based design approaches can now be clearly articulated. In the in-sample approach, the optimal parameters (Ω_d, ξ_d) are determined independently for each realisation of the uncertainty parameter χ, after which the resulting distributions are aggregated through statistical measures such as $E[(\Omega_d)^2(\chi)]$ and $E[\xi_d^2(\chi)]$. Consequently, the fixed points $r_{1,2}$ vary with χ, reflecting a locally optimal but uncertainty-dependent tuning strategy. In contrast, the ensemble-based approach seeks a single set of fixed points $r_{1,2}$ that satisfy distributional constraints, such as $E[y_1(\chi)] = E[y_2(\chi)]$, while also minimising the variance of the response. The corresponding damping ratio ξ_d is then computed based on these deterministic fixed points. Although both approaches ultimately yield a single set of design parameters (Ω_d^*, ξ_d^*), they arise from fundamentally different optimisation philosophies, one based on conditional optimality and the other on global robustness. The numerical results presented subsequently will demonstrate whether these differing design strategies lead to significantly distinct parameter selections and performance outcomes.

7. Dynamic response analysis

Having established the optimal damper parameters using both in-sample and ensemble-based formulations, it is now essential to assess how these designs influence the actual dynamic behaviour of the controlled system. While the preceding sections focused on parameter selection and robustness considerations, the effectiveness of these designs must ultimately be evaluated in terms of structural response reduction under excitation. In particular, examining the system response across a range of frequencies provides direct insight into resonance suppression, energy redistribution, and sensitivity to uncertainty. Therefore, the following subsection investigates the frequency domain characteristics of the controlled system, enabling a comparative assessment of the proposed design strategies in terms of their dynamic performance.

7.1. Frequency domain responses

Fig. 10 presents the Monte Carlo simulation (MCS)-based mean structural displacement response under frequency uncertainty, illustrating the effectiveness of different tuned mass damper (TMD) design strategies. The analysis is carried out for a fixed mass ratio of $\mu_d = 0.05$, with structural uncertainty characterised by $\epsilon = 0.10$. A total of 10,000 Monte Carlo samples are generated using Latin hypercube sampling to ensure an accurate representation of the stochastic space, and the response is evaluated over a frequency ratio range of $r \in [0,2]$. It should be noted that the classical tuning formulas proposed by Den Hartog were originally derived for a harmonically force-excited primary structure. In the present study, however, the structural system is subjected to base excitation, and all dynamic responses are evaluated using the governing equations and transfer functions derived for the ground-excited system in Eqs. (2) to (6). The Den Hartog solution is therefore employed only as a conventional deterministic benchmark design to provide a consistent benchmark for comparison with the proposed in-sample and ensemble optimisation frameworks. The primary objective of this work is to investigate the influence of structural uncertainty on TMD optimisation philosophies rather than to develop an excitation-specific tuning rule. Consequently, ground-motion-specific empirical tuning formulas available in the literature are not adopted, as their applicability depends on the characteristics of the assumed excitation and associated performance criteria. Using the classical Den Hartog design as a baseline enables a direct assessment of the benefits achieved by incorporating uncertainty explicitly within the optimisation process. The conventional TMD parameters are obtained from classical tuning relations [18], yielding $\Omega_d = \frac{1}{1+\mu_d} \approx 0.9524$ and $\xi_d = \sqrt{\frac{3\mu_d}{8(1+\mu_d)}} \approx 0.1336$. In contrast, the in-sample design employs $\Omega_d = 0.9512$ and $\xi_d = 0.1416$, while the ensemble-based design adopts $\Omega_d = 0.9225$ and $\xi_d = 0.1473$, reflecting the influence of uncertainty aware optimisation. In Fig. 10(a), the uncontrolled system exhibits a pronounced resonance peak, indicating strong

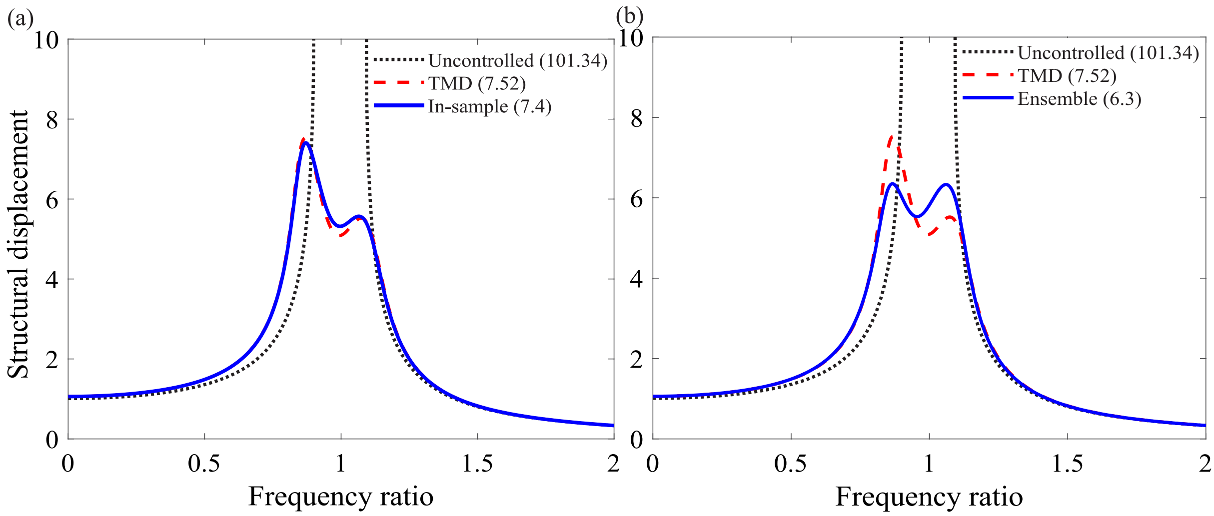

Fig. 10. Monte Carlo simulation (MCS)-based mean structural displacement response under frequency uncertainty $\epsilon = 0.1$ and $\mu_d = 0.05$. (a) Comparison of uncontrolled structure, conventional tuned mass damper (TMD), and in-sample design; (b) comparison of uncontrolled structure, conventional TMD, and ensemble design. The proposed designs effectively suppress the resonance peak and redistribute the response into two controlled peaks, with the ensemble design yielding the lowest maximum response.

amplification near the natural frequency. The introduction of a conventional TMD significantly reduces this peak and splits the response into two characteristic controlled peaks. The in-sample design further improves the response by slightly lowering the maximum amplitude and providing a more balanced distribution between the two peaks. However, the overall shape remains similar to that of the conventional TMD, suggesting that the in-sample approach retains a tuning behaviour close to the deterministic design. Fig. 10(b) shows the response corresponding to the ensemble-based design. A notable reduction in the maximum displacement is observed compared to both the conventional and in-sample cases. The response curve becomes smoother, and the two peaks are more evenly distributed, indicating a more effective redistribution of vibrational energy across the frequency range. This behaviour is consistent with the higher damping ratio and lower tuning frequency adopted in the ensemble design, which together enhance robustness against frequency variability. A comparison of the peak responses clearly highlights the performance hierarchy: the uncontrolled system yields the largest response, followed by the conventional TMD, then the in-sample design, while the ensemble-based design produces the lowest maximum displacement. This demonstrates that incorporating uncertainty directly into the design process leads to improved vibration mitigation. The maximum displacement of the uncontrolled structure is 101.34. The maximum displacement of the structure with the conventional tuned mass damper is 7.52. The maximum displacements of the structures with the in-sample and ensemble-based tuned mass dampers are obtained as 7.4 and 6.3, respectively. Accordingly, the in-sample and ensemble TMDs are 1.6% and 16.22% superior to the conventional TMD. These results clearly demonstrate the advantage of incorporating uncertainty into the design process, leading to improved vibration mitigation performance. In particular, the ensemble-based approach provides a more robust and reliable reduction in structural response under uncertain conditions. Overall, Fig. 10 confirms that while conventional and in-sample designs provide substantial reductions in resonance response, the ensemble-based approach offers superior robustness by systematically accounting for structural uncertainty. The results emphasise the importance of uncertainty aware tuning in achieving reliable vibration control performance across a population of structures. Fig. 11 further examines the robustness characteristics of the conventional deterministic TMD, the in-sample design, and the ensemble-based design by evaluating the variation of the peak normalised structural response with respect to structural frequency detuning. The horizontal axis represents the structural frequency error ratio varying from -10% to $+10\%$, while the vertical axis represents the corresponding maximum normalised structural response obtained from the frequency response function. This analysis provides a direct assessment of the sensitivity of each design methodology to uncertainty induced shifts in the dominant structural frequency. The conventional deterministic TMD exhibits a pronounced sensitivity to frequency mismatch. The response increases rapidly as the structural frequency deviates from the nominal tuning condition, particularly for negative detuning. This behaviour is characteristic of classically tuned absorbers, whose performance strongly depends on maintaining accurate resonance alignment between the primary structure and the absorber. When the structural frequency deviates from the nominal value, the fixed-point tuning condition shifts, resulting in a degradation of the vibration mitigation performance and an increase in resonance amplification. The in-sample design exhibits a response trend that remains close to the conventional deterministic TMD over the considered detuning range. This behaviour is consistent with the optimisation philosophy of the in-sample formulation, in which the absorber parameters are optimised conditionally for the nominal structural realisation. Consequently, the resulting tuning parameters remain close to the deterministic optimal solution, leading to similar off-nominal response characteristics. Although slight improvements in peak response reduction are observed, the overall sensitivity to structural frequency mismatch remains comparable to that of the conventional TMD. This observation is also consistent with the parameter comparisons presented previously, where the in-sample design produced frequency and damping ratios close to the deterministic solution. In contrast, the ensemble-based design demonstrates substantially different robustness characteristics. The ensemble optimisation produces a smoother and less sharply varying response curve over the uncertainty range, indicating reduced sensitivity to structural frequency deviations. In particular, the ensemble-based design significantly suppresses the peak response under negative detuning conditions, where the conventional and in-sample designs experience severe amplification. This improved robustness arises because the ensemble formulation incorporates uncertainty directly into the optimisation process by minimising distributional response measures rather than enforcing local optimality for a single structural realisation. As a result, the ensemble design intentionally shifts the absorber tuning towards lower frequency ratios and higher damping values, thereby broadening the effective operational bandwidth of the vibration absorber and reducing resonance sensitivity. The asymmetric behaviour of the ensemble-based response under positive and negative frequency deviations can be attributed to the distributional optimisation framework adopted

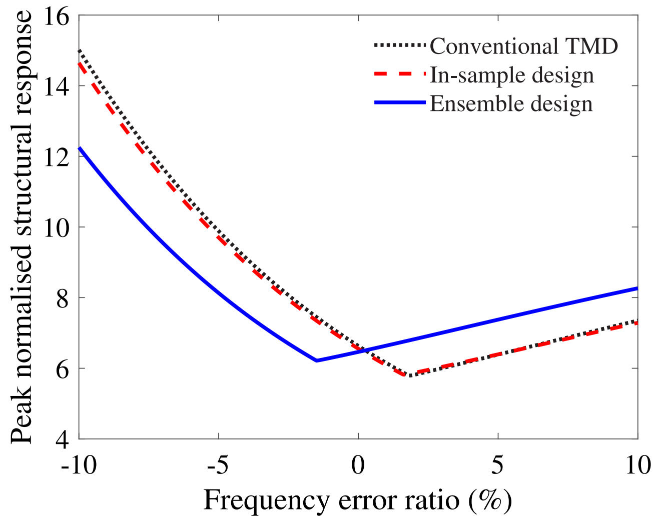

Fig. 11. Variation of the peak normalised structural response with respect to the frequency error ratio for the conventional tuned mass damper (TMD), in-sample design, and ensemble-based design. The ensemble-based design exhibits improved robustness against frequency detuning and uncertainty-induced off-nominal structural conditions, resulting in reduced sensitivity to negative frequency deviations and a smoother overall response variation.

in the present study. Unlike deterministic fixed-point tuning, the ensemble-based formulation minimises the expected stochastic response over the entire uncertainty domain rather than enforcing optimality at every individual detuning realisation. Consequently, the optimisation process sacrifices local optimality near certain positive detuning conditions in exchange for improved global robustness and reduced sensitivity across the overall stochastic parameter space. This trade-off is characteristic of robust optimisation strategies, where a moderate increase in response under some local conditions is accepted to achieve a more reliable and stable performance under uncertainty. It should be noted that a frequency error ratio of zero corresponds to the nominal tuning condition, where the actual structural frequency coincides with the frequency assumed during the design process. For conventionally tuned absorbers, the optimal performance is generally expected near this nominal condition. However, owing to the coupled absorber-structure dynamics and the adopted peak-response performance measure, the minimum response does not necessarily occur exactly at zero frequency error and may shift slightly within the vicinity of the nominal tuning condition. This behaviour is also consistent with the smoother response variation and reduced sensitivity to off-nominal structural frequencies observed for the ensemble-based design. Overall, the results presented in Fig. 11 clearly demonstrate the fundamental distinction between conditional optimisation and distributional robustness in uncertainty-informed TMD design. While the conventional deterministic and in-sample approaches provide effective vibration suppression near the nominal tuning condition, the ensemble-based design offers improved robustness against structural frequency variability and uncertainty-induced detuning effects. These observations further confirm the advantages of incorporating uncertainty directly into the absorber optimisation process for achieving reliable vibration mitigation performance under uncertain structural conditions.

7.2. Time domain responses

The time domain responses are obtained by recasting the coupled second order equations of motion into a first order state space representation, which is subsequently integrated using a high order explicit Runge Kutta scheme. This approach enables accurate and stable computation of the transient structural response under base excitation while preserving the coupled dynamics of the primary system and the absorber. Eq. (2) is further utilised to perform this time domain analysis. Accordingly, a convenient matrix form is derived from Eq. (2) and expressed as

$$\mathbf{M}\ddot{\mathbf{u}} + \mathbf{C}\dot{\mathbf{u}} + \mathbf{K}\mathbf{u} = \mathbf{f}(t) \tag{78}$$

The mass, damping, stiffness, and force matrices are derived as

$$\mathbf{u}(t) = \begin{bmatrix} u_s \\ u_d \end{bmatrix}, \mathbf{f}(t) = \begin{bmatrix} -m_s\ddot{u}_g \\ -m_d\ddot{u}_g \end{bmatrix}, \mathbf{M} = \begin{bmatrix} m_s & 0 \\ m_d & m_d \end{bmatrix}, \mathbf{C} = \begin{bmatrix} c_s & -c_d \\ 0 & c_d \end{bmatrix}, \mathbf{K} = \begin{bmatrix} k_s & -k_d \\ 0 & k_d \end{bmatrix} \tag{79}$$

The second order time domain equation is further developed and expressed as

$$\ddot{\mathbf{u}} = \mathbf{M}^{-1}\left(\mathbf{f}(t) - \mathbf{C}\dot{\mathbf{u}} - \mathbf{K}\mathbf{u}\right) \tag{80}$$

where the acceleration of the main structure is derived as

$$\ddot{u}_s = -\frac{c_s}{m_s}\dot{u}_s - \frac{k_s}{m_s}u_s + \frac{c_d}{m_s}\dot{u}_d + \frac{k_d}{m_s}u_d - \ddot{u}_g \tag{81}$$

The second expression of Eq. (2) is utilised further to derive the acceleration of the damper and expressed as

$$\ddot{u}_d = -\ddot{u}_s - \frac{c_d}{m_d}\dot{u}_d - \frac{k_d}{m_d}u_d - \ddot{u}_g \tag{82}$$

Eq. (82) substitutes in Eq. (81) and the acceleration of the damper is derived as

$$\ddot{u}_d = \frac{c_s}{m_s}\dot{u}_s + \frac{k_s}{m_s}u_s - \left(\frac{c_d}{m_s} + \frac{c_d}{m_d}\right)\dot{u}_d - \left(\frac{k_d}{m_s} + \frac{k_d}{m_d}\right)u_d \tag{83}$$

Accordingly, the accelerations of the primary structure and damper are derived as

$$\begin{aligned}\ddot{u}_s &= -\frac{c_s}{m_s}\dot{u}_s - \frac{k_s}{m_s}u_s + \frac{c_d}{m_s}\dot{u}_d + \frac{k_d}{m_s}u_d - \ddot{u}_g \\ \ddot{u}_d &= \frac{c_s}{m_s}\dot{u}_s + \frac{k_s}{m_s}u_s - \left(\frac{c_d}{m_s} + \frac{c_d}{m_d}\right)\dot{u}_d - \left(\frac{k_d}{m_s} + \frac{k_d}{m_d}\right)u_d\end{aligned} \tag{84}$$

The state vectors are derived as

$$\dot{\mathbf{x}} = \begin{bmatrix}\dot{u}_s \\ \dot{u}_d \\ \ddot{u}_s \\ \ddot{u}_d\end{bmatrix} = \begin{bmatrix} x_3 \\ x_4 \\ -\frac{c_s}{m_s}x_3 - \frac{k_s}{m_s}x_1 + \frac{c_d}{m_s}x_4 + \frac{k_d}{m_s}x_2 - \ddot{u}_g \\ \frac{c_s}{m_s}x_3 + \frac{k_s}{m_s}x_1 - \left(\frac{c_d}{m_s} + \frac{c_d}{m_d}\right)x_4 - \left(\frac{k_d}{m_s} + \frac{k_d}{m_d}\right)x_2 \end{bmatrix} \tag{85}$$

where $\ddot{u}_g$ is considered as

$$\ddot{u}_g = A_g \sin \omega_g t \tag{86}$$

The values of A_g and ω_g are considered as

$$A_g = 0.1 \quad \text{and} \quad \omega_g = 1.2\omega_{s0} \tag{87}$$

Fig. 12 presents the time domain displacement responses of the controlled structure under uncertainty, comparing the in-sample and ensemble-based designs. The results include individual random realisations, the deterministic response, and the Monte Carlo simulation (MCS) mean, providing a clear view of the transient and steady state behaviour. In Fig. 12(a), corresponding to the in-sample design, the structural response shows noticeable variability during both the transient and steady state phases. The random realisations exhibit a wide spread in amplitude, particularly in the early stages of motion, indicating sensitivity to uncertainty in the system parameters. Although the oscillations gradually stabilise over time, the amplitude remains moderately dispersed. The deterministic response follows a smoother trajectory but does not fully capture the extent of this variability. The MCS mean curve lies centrally within the random band and provides a representative estimate of the overall response. However, the persistence of relatively large oscillation amplitudes suggests that the in-sample design only partially mitigates the effects of uncertainty. In contrast, Fig. 12(b) shows the response for the ensemble-based design. A more uniform and controlled behaviour is observed, with the spread of the random realisations becoming more symmetric and less irregular compared to the in-sample case. The oscillation amplitudes are more consistently regulated over time, and the response exhibits improved stability in the steady state region. The MCS mean closely follows the deterministic curve, indicating reduced sensitivity to parameter variability. This reflects the inherent robustness of the ensemble design, which incorporates uncertainty directly into the tuning process. Overall, Fig. 12 demonstrates that while both designs are effective in controlling the structural response, the ensemble-based approach provides superior performance in the time domain by reducing variability and ensuring more consistent oscillation amplitudes. These results reinforce the conclusions drawn from the frequency domain analysis, highlighting the advantage of uncertainty aware design in achieving stable and reliable dynamic behaviour. Fig. 13 presents the time-domain displacement responses of the structure under uncertainty, comparing the uncontrolled system, the conventional tuned mass damper (TMD), and the proposed designs. The results highlight the effectiveness of the control strategies in mitigating vibrations over time. In Fig. 13(a), corresponding to the in-sample design, the uncontrolled response exhibits large and irregular oscillations, reflecting the strong influence of uncertainty on the structural dynamics. The conventional TMD reduces the amplitude to some extent; however, noticeable fluctuations and intermittent amplification remain, particularly during certain time intervals. The in-sample design provides a more stable response, with reduced peak amplitudes and a smoother oscillation pattern compared to both the uncontrolled and conventional cases. Nevertheless, some variability persists, indicating that the in-sample approach only partially accounts for the effects of uncertainty. In Fig. 13(b), the ensemble-based design demonstrates a more pronounced improvement. The oscillations are more uniform and consistently controlled throughout the time history. Compared to the conventional TMD, the ensemble design achieves a clearer reduction in amplitude and avoids the irregular amplification observed in the uncontrolled response. The response appears more balanced and less sensitive to fluctuations, indicating enhanced robustness. The improvement over the in-sample design is also evident, as the ensemble approach maintains more consistent oscillation amplitudes and reduces variability over the entire time range. The maximum MCS displacement of the uncontrolled structure is 0.342966 m, whereas the corresponding maximum displacements of the structures with the conventional, in-sample, and ensemble-based tuned mass dampers are 0.339172 m, 0.273637 m, and 0.266219 m, respectively. With respect to the conventional TMD, the vibration reduction capacities of the in-sample and ensemble TMDs are 19.32% and 21.50%, respectively. These results indicate that both uncertainty informed designs outperform the conventional TMD in the time domain, with the ensemble-based design providing the greatest reduction in peak structural response. Overall, Fig. 13 confirms that both proposed designs outperform the conventional TMD in controlling structural vibrations under uncertainty. Among them, the ensemble-based design provides the most reliable performance, delivering a more uniform and stable response in the time domain. These observations are consistent with the frequency domain results, reinforcing the advantage of incorporating uncertainty directly into the design process.

8. Conclusion

This paper has introduced a unified analytical framework for the optimal design of tuned mass dampers under structural frequency uncertainty by systematically distinguishing between in-sample and ensemble-based optimisation philosophies. Unlike conventional deterministic tuned mass damper (TMD) design approaches, the proposed framework explicitly recognises that the optimality of vibration absorbers depends fundamentally on how uncertainty is incorporated into the optimisation process. The results demonstrate that uncertainty-informed TMD optimisation is not merely a stochastic extension of deterministic tuning methods, but rather a conceptually distinct optimisation problem requiring explicit consideration of conditional versus distributional optimality. The major findings and contributions of this paper are summarised as follows:

- A unified analytical framework has been developed to systematically distinguish between in-sample and ensemble-based optimal TMD design philosophies under structural frequency uncertainty.

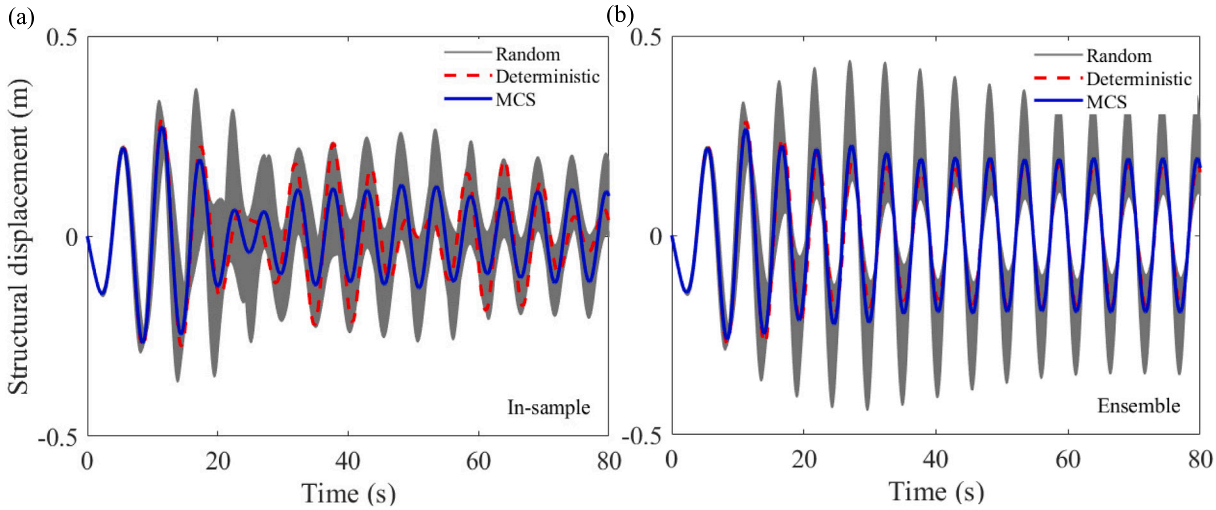

Fig. 12. The variations of displacements of the structures equipped with tuned mass damper with respect to time, comparing (a) in-sample and (b) ensemble-based optimal designs. The graph includes random, deterministic, and MCS plots in the design.

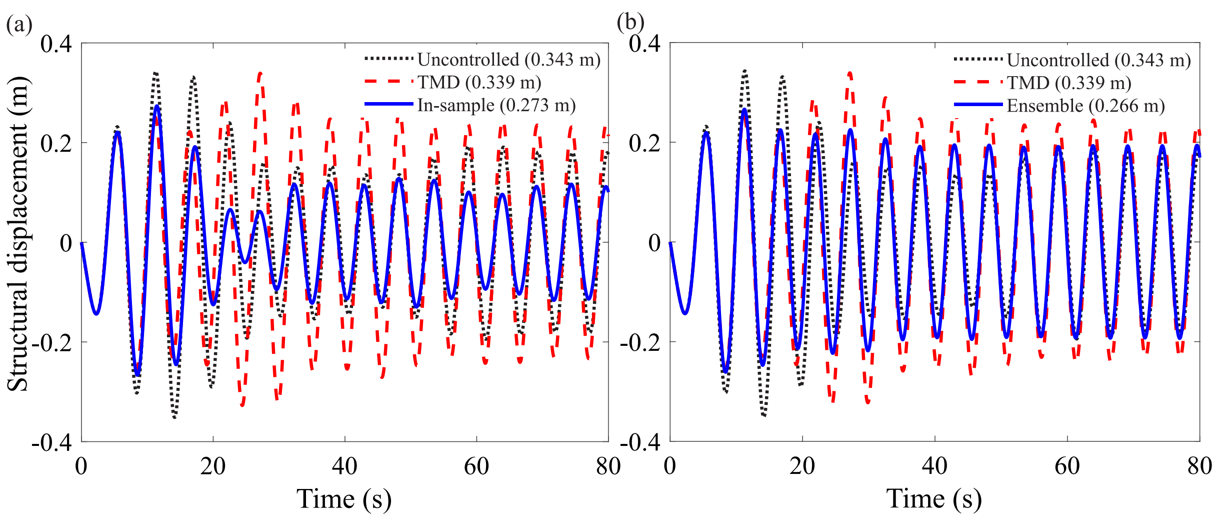

Fig. 13. The variations of the mean structural displacements of the structures equipped with tuned mass dampers with respect to time, obtained using Monte Carlo simulation (MCS), comparing (a) in-sample and (b) ensemble-based optimal designs. The responses of the uncontrolled structure and the structure with a conventional tuned mass damper (TMD) are also included for comparison.

- Closed-form analytical expressions have been derived for the optimal tuning frequency ratios and damping ratios corresponding to both optimisation strategies under uncertain structural conditions.
- The in-sample optimisation approach produces optimal parameters conditional on individual structural realisations and is therefore more suitable for adaptive, retunable, or custom-calibrated TMD systems.
- The ensemble-based optimisation systematically shifts the optimal design towards lower tuning frequency ratios and higher damping ratios, thereby broadening the operational bandwidth and improving robustness against uncertainty-induced frequency detuning effects.
- Monte Carlo simulations in both frequency and time domains validate the analytical framework and demonstrate that the ensemble-based design achieves approximately 21.50% reduction in the structural displacement response compared with the conventional TMD design, whereas the in-sample optimisation achieves approximately 19.32% reduction.
- The ensemble-based design exhibits substantially improved robustness and reduced sensitivity to parameter variability across stochastic realisations, confirming the effectiveness of the distributional optimisation philosophy for fixed and mass-produced vibration absorber applications.
- The proposed framework establishes a transferable uncertainty-aware optimisation methodology applicable to broader vibration control systems under parametric uncertainty.

The results further indicate that the selection of the optimisation philosophy is closely associated with practical considerations such as information availability, implementation strategies, manufacturing constraints, and robustness requirements. Beyond the specific TMD application considered in this study, the proposed framework may be extended to a broad class of uncertain structural control problems in which system properties are random while the control parameters remain fixed. The principal novelty of this work lies in establishing a unified analytical framework that systematically distinguishes between conditional optimality and distributional robustness under uncertainty, thereby providing a new perspective for the design of vibration control systems beyond conventional deterministic and stochastic optimisation approaches. Although the present study considers an uncertain SDOF structure, the proposed optimisation framework is not restricted to SDOF systems and can be extended to MDOF structures through modal decomposition or reduced-order modelling techniques. However, the optimal TMD parameters obtained for the present SDOF system cannot be directly applied to a general MDOF structure, as they depend on the modal characteristics, uncertainty distributions, and performance objectives of the specific system under consideration. Additional investigations incorporating stochastic excitation models, non-Gaussian uncertainty distributions, and experimental validations may further enhance the applicability of the proposed methodology to practical engineering vibration control systems. The present study focuses on harmonic base excitation to enable analytical development and systematic comparison of the proposed optimisation frameworks. Future research may extend the methodology to non-stationary earthquake records and seismic performance assessment of controlled structures.

CRediT authorship contribution statement

Sudip Chowdhury: Writing – review & editing, Writing – original draft, Visualization, Validation, Software, Resources, Project administration, Methodology, Investigation, Funding acquisition, Formal analysis, Data curation, Conceptualization. **Sondipon Adhikari:** Writing – review & editing, Writing – original draft, Visualization, Validation, Supervision, Methodology, Investigation, Conceptualization.

Declaration of competing interest

The authors declare that they have no known competing financial interests or personal relationships that could have appeared to influence the work reported in this paper.

Acknowledgements

The authors would like to acknowledge the Post Doctoral grant received from The University of Glasgow during the period of this research work.

Appendix. The closed-form expressions from Eqs. (14), (16), (17), (23), and (36)

The closed-form expressions for G_3, G_4, G_5, and G_6 from Eq. (14) are listed below.

$$G_3 = \begin{array}{c} 4\left(\left(\xi_s^2-\frac{1}{2}\right)r^4+\left(\frac{1}{2}+\left(-\xi_s^2+\frac{\mu_d}{2}+\frac{1}{2}\right)\Omega_d^2\right)r^2-\frac{\Omega_d^2}{2}\right)\varepsilon\left(r-\Omega_d\right)\left(r+\Omega_d\right)\sqrt{3} \\ +r^8+\left(\left(-2\mu_d-2\right)\Omega_d^2+4\xi_s^2-2\right)r^6 \\ +\left(\left(\mu_d+1\right)^2\Omega_d^4+\left(-8\xi_s^2+2\mu_d+4\right)\Omega_d^2+3\varepsilon^2+1\right)r^4 \\ -2\left(\left(-2\xi_s^2+\mu_d+1\right)\Omega_d^2+3\varepsilon^2+1\right)\Omega_d^2r^2+\Omega_d^4\left(3\varepsilon^2+1\right) \end{array} \tag{A.1}$$

$$G_4 = \begin{array}{c} 4\left(\left(\xi_s^2-\frac{1}{2}\right)r^4+\left(\frac{1}{2}+\left(-\xi_s^2+\frac{\mu_d}{2}+\frac{1}{2}\right)\Omega_d^2\right)r^2-\frac{\Omega_d^2}{2}\right)\varepsilon\left(r-\Omega_d\right)\left(r+\Omega_d\right)\sqrt{3} \\ -r^8+\left(\left(2\mu_d+2\right)\Omega_d^2-4\xi_s^2+2\right)r^6 \\ +\left(-\left(\mu_d+1\right)^2\Omega_d^4+\left(8\xi_s^2-2\mu_d-4\right)\Omega_d^2-3\varepsilon^2-1\right)r^4 \\ +2\left(\left(-2\xi_s^2+\mu_d+1\right)\Omega_d^2+3\varepsilon^2+1\right)\Omega_d^2r^2+\left(-3\varepsilon^2-1\right)\Omega_d^4 \end{array} \tag{A.2}$$

$$G_5 = 2\left(\begin{array}{c} \frac{\varepsilon\left(r^2-\Omega_d^2\right)\sqrt{3}}{2}+\left(\xi_s^2-\frac{1}{2}\right)r^4 \\ +\left(\frac{1}{2}+\left(-\xi_s^2+\frac{\mu_d}{2}+\frac{1}{2}\right)\Omega_d^2\right)r^2-\frac{\Omega_d^2}{2} \end{array}\right)\varepsilon\left(r-\Omega_d\right)\left(r+\Omega_d\right) \tag{A.3}$$

$$G_6 = \left(\begin{array}{c} -2r^4\xi_s^2+2r^2\Omega_d^2\xi_s^2+\sqrt{3}\,\varepsilon r^2-\sqrt{3}\,\Omega_d^2\varepsilon+r^4 \\ -r^2\Omega_d^2-r^2+\Omega_d^2-r^2\Omega_d^2\mu_d \end{array}\right)\left(r+\Omega_d\right)\left(r-\Omega_d\right)\varepsilon \tag{A.4}$$

The closed-form expression for N_s is derived as

$$N_s = \arctan\left(\frac{\varepsilon\left(\begin{array}{c} -2r^6\xi_s^2+4r^4\xi_s^2\Omega_d^2-2r^2\xi_s^2\Omega_d^4-\mu_d r^4\Omega_d^2 \\ +\mu_d r^2\Omega_d^4+\sqrt{3}\,r^4\varepsilon-2\sqrt{3}\,r^2\Omega_d^2\varepsilon+\sqrt{3}\,\Omega_d^4\varepsilon \\ +r^6-2r^4\Omega_d^2+r^2\Omega_d^4-r^4+2r^2\Omega_d^2-\Omega_d^4 \end{array}\right)}{2\sqrt{-r^4\xi_s^2\varepsilon^2\left(r^2-\Omega_d^2\right)^3\left(r^2\xi_s^2-\Omega_d^2\xi_s^2+\mu_d\Omega_d^2-r^2+\Omega_d^2\right)}}\right) + \arctan\left(\frac{\varepsilon\left(\begin{array}{c} 2r^6\xi_s^2-4r^4\xi_s^2\Omega_d^2+2r^2\xi_s^2\Omega_d^4+\mu_d r^4\Omega_d^2 \\ -\mu_d r^2\Omega_d^4+\sqrt{3}\,r^4\varepsilon-2\sqrt{3}\,r^2\Omega_d^2\varepsilon+\sqrt{3}\,\Omega_d^4\varepsilon \\ -r^6+2r^4\Omega_d^2-r^2\Omega_d^4+r^4-2r^2\Omega_d^2+\Omega_d^4 \end{array}\right)}{2\sqrt{-r^4\xi_s^2\varepsilon^2\left(r^2-\Omega_d^2\right)^3\left(r^2\xi_s^2-\Omega_d^2\xi_s^2+\mu_d\Omega_d^2-r^2+\Omega_d^2\right)}}\right) \tag{A.5}$$

The closed-form expressions for W, Y, Z, G_1, G_2, and V from Eq. (17) are listed below.

$$W = \left(\xi_s^2 - \frac{1}{4}\right) r^2 + \frac{\Omega_d^2\left(-4\xi_s^2 + \mu_d + 1\right)}{4} \tag{A.6}$$

$$V = \sqrt{-r^4\xi_s^2\epsilon^2\left(r^2 - \Omega_d^2\right)^3\left(r^2\xi_s^2 - \Omega_d^2\xi_s^2 + \mu_d\Omega_d^2 - r^2 + \Omega_d^2\right)} \tag{A.7}$$

$$G_1 = \begin{array}{c} -4\sqrt{3}\, r^2\Omega_d^2\epsilon + 4\sqrt{3}\,\Omega_d^2\epsilon\, r^4 + 2\sqrt{3}\,\mu_d r^4\Omega_d^2\epsilon - 2\sqrt{3}\,\mu_d r^2\Omega_d^4\epsilon - 8\sqrt{3}\, r^4\xi_s^2\Omega_d^2\epsilon \\ +4\sqrt{3}\, r^2\xi_s^2\Omega_d^4\epsilon + 4r^2\xi_s^2\Omega_d^4 + 2\mu_d r^4\Omega_d^2 - 8r^4\xi_s^2\Omega_d^2 - 2\sqrt{3}\, r^6\epsilon - 2\sqrt{3}\,\Omega_d^4\epsilon\, r^2 \\ +4\sqrt{3}\, r^6\xi_s^2\epsilon + 2\sqrt{3}\,\Omega_d^4\epsilon + 2\sqrt{3}\, r^4\epsilon - 2\mu_d r^2\Omega_d^4 - 2r^2\Omega_d^4 + 4r^6\xi_s^2 + 4r^4\Omega_d^2 \\ -2r^2\Omega_d^2 + \Omega_d^4 - 2r^6 + r^4 + r^8 + 3\epsilon^2 r^4 - 2r^6\Omega_d^2 + r^4\Omega_d^4 + 3\epsilon^2\Omega_d^4 + 2\mu_d r^4\Omega_d^4 \\ +\mu_d^2 r^4\Omega_d^4 - 2\mu_d r^6\Omega_d^2 - 6\epsilon^2\Omega_d^2 r^2 \end{array} \tag{A.8}$$

$$G_2 = \begin{array}{c} 4\sqrt{3}\, r^2\Omega_d^2\epsilon - 4\sqrt{3}\,\Omega_d^2\epsilon\, r^4 - 2\sqrt{3}\,\mu_d r^4\Omega_d^2\epsilon + 2\sqrt{3}\,\mu_d r^2\Omega_d^4\epsilon + 8\sqrt{3}\, r^4\xi_s^2\Omega_d^2\epsilon \\ -4\sqrt{3}\, r^2\xi_s^2\Omega_d^4\epsilon + 4r^2\xi_s^2\Omega_d^4 + 2\mu_d r^4\Omega_d^2 - 8r^4\xi_s^2\Omega_d^2 + 2\sqrt{3}\, r^6\epsilon + 2\sqrt{3}\,\Omega_d^4\epsilon\, r^2 \\ -4\sqrt{3}\, r^6\xi_s^2\epsilon - 2\sqrt{3}\,\Omega_d^4\epsilon - 2\sqrt{3}\, r^4\epsilon - 2\mu_d r^2\Omega_d^4 - 2r^2\Omega_d^4 + 4r^6\xi_s^2 + 4r^4\Omega_d^2 \\ -2r^2\Omega_d^2 + \Omega_d^4 - 2r^6 + r^4 + r^8 + 3\epsilon^2 r^4 - 2r^6\Omega_d^2 + r^4\Omega_d^4 + 3\epsilon^2\Omega_d^4 + 2\mu_d r^4\Omega_d^4 \\ +\mu_d^2 r^4\Omega_d^4 - 2\mu_d r^6\Omega_d^2 - 6\epsilon^2\Omega_d^2 r^2 \end{array} \tag{A.9}$$

$$Y = \frac{\epsilon\left(\begin{array}{c} 2r^6\xi_s^2 - 4r^4\xi_s^2\Omega_d^2 + 2r^2\xi_s^2\Omega_d^4 + \mu_d r^4\Omega_d^2 - \mu_d r^2\Omega_d^4 + \sqrt{3}\, r^4\epsilon \\ -2\sqrt{3}\, r^2\Omega_d^2\epsilon + \sqrt{3}\,\Omega_d^4\epsilon - r^6 + 2r^4\Omega_d^2 - r^2\Omega_d^4 + r^4 - 2r^2\Omega_d^2 + \Omega_d^4 \end{array}\right)}{2\sqrt{-r^4\xi_s^2\epsilon^2\left(r^2 - \Omega_d^2\right)^3\left(r^2\xi_s^2 - \Omega_d^2\xi_s^2 + \mu_d\Omega_d^2 - r^2 + \Omega_d^2\right)}} \tag{A.10}$$

$$Z = \frac{\epsilon\left(\begin{array}{c} -2r^6\xi_s^2 + 4r^4\xi_s^2\Omega_d^2 - 2r^2\xi_s^2\Omega_d^4 - \mu_d r^4\Omega_d^2 + \mu_d r^2\Omega_d^4 + \sqrt{3}\, r^4\epsilon \\ -2\sqrt{3}\, r^2\Omega_d^2\epsilon + \sqrt{3}\,\Omega_d^4\epsilon + r^6 - 2r^4\Omega_d^2 + r^2\Omega_d^4 - r^4 + 2r^2\Omega_d^2 - \Omega_d^4 \end{array}\right)}{2\sqrt{-r^4\xi_s^2\epsilon^2\left(r^2 - \Omega_d^2\right)^3\left(r^2\xi_s^2 - \Omega_d^2\xi_s^2 + \mu_d\Omega_d^2 - r^2 + \Omega_d^2\right)}} \tag{A.11}$$

$$N_1 = \begin{array}{l} \arctan\left(\dfrac{\begin{array}{c} 4\mu_d r^4\xi_d^2\Omega_d^2 + 4\sqrt{3}\, r^2\xi_d^2\Omega_d^2\epsilon + 4r^4\xi_d^2\Omega_d^2 - \mu_d r^4\Omega_d^2 + \mu_d r^2\Omega_d^4 \\ +\sqrt{3}\, r^4\epsilon - 2\sqrt{3}\, r^2\Omega_d^2\epsilon + \sqrt{3}\,\Omega_d^4\epsilon + r^6 - 2r^4\Omega_d^2 - 4r^2\xi_d^2\Omega_d^2 \\ +r^2\Omega_d^4 - r^4 + 2r^2\Omega_d^2 - \Omega_d^4 \end{array}}{2\mu_d r^5\xi_d\Omega_d}\right) \\ +\arctan\left(\dfrac{\begin{array}{c} -4\mu_d r^4\xi_d^2\Omega_d^2 + 4\sqrt{3}\, r^2\xi_d^2\Omega_d^2\epsilon - 4r^4\xi_d^2\Omega_d^2 + \mu_d r^4\Omega_d^2 \\ +\sqrt{3}\, r^4\epsilon - 2\sqrt{3}\, r^2\Omega_d^2\epsilon + \sqrt{3}\,\Omega_d^4\epsilon - r^6 + 2r^4\Omega_d^2 \\ +4r^2\xi_d^2\Omega_d^2 - r^2\Omega_d^4 + r^4 - 2r^2\Omega_d^2 + \Omega_d^4 - \mu_d r^2\Omega_d^4 \end{array}}{2\mu_d r^5\xi_d\Omega_d}\right) \end{array} \tag{A.12}$$

The closed-form expressions for Z_2, Z_1, and Z_0 from Eq. (36) are listed below.

$$Z_2 = -32r_{1,2}^4\Omega_d^4\left(\mu_d + 1\right)^3\left(-\chi\epsilon + \mu_d r_{1,2}^2 + r_{1,2}^2 - 1\right) \tag{A.13}$$

$$Z_1 = \begin{array}{c} \left(-16\mu_d^2\Omega_d^2 - 32\mu_d\Omega_d^2 - 16\Omega_d^2\right) r_{1,2}^8 \\ +\left(\begin{array}{c} 32\mu_d^3\Omega_d^4 + 16\mu_d^2\chi\,\Omega_d^2\epsilon + 96\mu_d^2\Omega_d^4 + 32\chi\mu_d\Omega_d^2\epsilon \\ +96\mu_d\Omega_d^4 + 16\chi\,\Omega_d^2\epsilon + 16\mu_d^2\Omega_d^2 + 32\Omega_d^4 + 32\mu_d\Omega_d^2 + 16\Omega_d^2 \end{array}\right) r_{1,2}^6 \\ +\left(\begin{array}{c} -16\mu_d^4\Omega_d^6 - 8\chi\,\mu_d^3\Omega_d^4\epsilon - 64\mu_d^3\Omega_d^6 - 4\epsilon^2\chi^2\mu_d^2\Omega_d^2 - 48\chi\,\mu_d^2\Omega_d^4\epsilon \\ -96\mu_d^2\Omega_d^6 - 8\epsilon^2\chi^2\mu_d\Omega_d^2 - 72\chi\mu_d\Omega_d^4\epsilon - 8\mu_d^3\Omega_d^4 - 64\mu_d\Omega_d^6 \\ -8\mu_d^2\chi\,\Omega_d^2\epsilon - 32\chi\,\Omega_d^4\epsilon - 48\mu_d^2\Omega_d^4 - 16\Omega_d^6 - 16\chi\mu_d\Omega_d^2\epsilon \\ -72\mu_d\Omega_d^4 - 4\mu_d^2\Omega_d^2 - 32\Omega_d^4 - 8\mu_d\Omega_d^2 \end{array}\right) r_{1,2}^4 \\ +\left(\begin{array}{c} 16\chi\,\mu_d^3\Omega_d^6\epsilon + 48\chi\,\mu_d^2\Omega_d^6\epsilon + 48\chi\mu_d\Omega_d^6\epsilon + 16\mu_d^3\Omega_d^6 \\ +16\chi\,\Omega_d^6\epsilon + 48\mu_d^2\Omega_d^6 + 48\mu_d\Omega_d^6 + 16\Omega_d^6 \end{array}\right) r_{1,2}^2 \end{array} \tag{A.14}$$

$$Z_0 = \begin{array}{c} -2\left(\left(-1 - \mu_d\right)\Omega_d^2 + r_{1,2}^2\right) \\ \left(\left(\mu_d + 1\right)^2\Omega_d^4 + \left(\chi\mu_d\epsilon - 2\mu_d r_{1,2}^2 + \mu_d - 2r_{1,2}^2\right)\Omega_d^2 + r_{1,2}^4\right) \\ \left(\left(\left(-1 - \mu_d\right) r_{1,2}^2 + \chi\epsilon + 1\right)\Omega_d^2 + \left(-\chi\epsilon + r_{1,2}^2 - 1\right) r_{1,2}^2\right) \end{array} \tag{A.15}$$

Data availability

All data, models, and code generated or used during the study appear in the submitted article.

References

[1] X. Su, H. Kang, T. Guo, Y. Cong, Internal resonance and energy transfer of a cable-stayed beam with a tuned mass damper, Nonlinear Dynam. 110 (1) (2022) 131–152.
[2] R. Wu, J. Yan, L. Xu, J. Liu, A. Guo, Experimental study on the dynamic response characteristics of the floating bridge considering pontoon failure under the combined action of earthquakes and waves, Earthq. Eng. Struct. Dyn. 55 (1) (2026) 112–129.
[3] Y. Li, S. Li, P. Tan, A novel tuned mass damper inerter: Optimal design, effectiveness comparison, and robustness investigation, Structures 55 (2023) 1262–1276.
[4] Z. Sun, D. Feng, H. Shi, D. Sun, Bayesian optimization of tuned mass damper for vibration control of the suspension footbridge with human–vehicle–bridge interaction, J. Vib. Control (2025) 10775463251343929.
[5] N. Su, J. Bian, S. Peng, Z. Chen, Y. Xia, Balancing static and dynamic performances of TMD with negative stiffness, Int. J. Mech. Sci. 243 (2023) 108068.
[6] H. Cetin, E. Aydin, B. Ozturk, Multiple tuned mass damper design for the mitigation of cantilever beam response, ASCE-ASME J. Risk Uncertain. Eng. Syst. Part A: Civ. Eng. 11 (3) (2025) 04025052.
[7] N. Su, Z. Chen, Y. Xia, J. Bian, Hybrid analytical H-norm optimization approach for dynamic vibration absorbers, Int. J. Mech. Sci. 264 (2024) 108796.
[8] J.P. Den Hartog, Mechanical Vibrations, Courier Corporation, 1985.
[9] P. Sun, Y. Peng, Reliability-informed design table for optimizing tuned mass-damper-inerter systems to improve structural seismic performance, Probabilistic Eng. Mech. 80 (2025) 103769.
[10] S. Krenk, Frequency analysis of the tuned mass damper, 2005.
[11] J. Høgsberg, B. Lossouarn, J.-F. Deü, Tuning of vibration absorbers by an effective modal coupling factor, Int. J. Mech. Sci. 268 (2024) 109009.
[12] G.C. Marano, R. Greco, S. Sgobba, A comparison between different robust optimum design approaches: Application to tuned mass dampers, Probabilistic Eng. Mech. 25 (1) (2010) 108–118.
[13] S. Chakraborty, B.K. Roy, Reliability based optimum design of tuned mass damper in seismic vibration control of structures with bounded uncertain parameters, Probabilistic Eng. Mech. 26 (2) (2011) 215–221.
[14] E. Mrabet, M. Guedri, M. Ichchou, S. Ghanmi, Stochastic structural and reliability based optimization of tuned mass damper, Mech. Syst. Signal Process. 60 (2015) 437–451.
[15] H. Yu, F. Gillot, M. Ichchou, Reliability based robust design optimization for tuned mass damper in passive vibration control of deterministic/uncertain structures, J. Sound Vib. 332 (9) (2013) 2222–2238.
[16] D. Li, H. Tang, S. Xue, Robust design of tuned mass damper with hybrid uncertainty, Struct. Control. Health Monit. 28 (10) (2021) e2803.
[17] I. Venanzi, Robust optimal design of tuned mass dampers for tall buildings with uncertain parameters, Struct. Multidiscip. Optim. 51 (1) (2015) 239–250.
[18] J. Ormondroyd, J. Den Hartog, The theory of the dynamic vibration absorber, Trans. Am. Soc. Mech. Eng. 49 (2) (1928) 021007.
[19] S. Chowdhury, A. Banerjee, The impacting vibration absorbers, Appl. Math. Model. 127 (2024) 454–505.
[20] C.-L. Lee, Y.-T. Chen, L.-L. Chung, Y.-P. Wang, Optimal design theories and applications of tuned mass dampers, Eng. Struct. 28 (1) (2006) 43–53.
[21] A. Batou, S. Adhikari, Optimal parameters of viscoelastic tuned-mass dampers, J. Sound Vib. 445 (2019) 17–28.
[22] M. Argenziano, A. Palmeri, A.R. Carotenuto, E. Mele, M. Fraldi, Optimization of viscoelastic tuned mass damper systems subjected to coloured excitations, Earthq. Eng. Struct. Dyn. 54 (12) (2025) 3244–3264.
[23] S. Chowdhury, R. Debbarma, S. Adhikari, Tuned inerter viscoelastic liquid column dampers, J. Sound Vib. (2025) 119319.
[24] P. Li, J. Zhang, Identification and uncertainty quantification of structural flexibility for reliability analysis, Mech. Syst. Signal Process. 163 (2022) 108104.
[25] S. Adhikari, M. Friswell, K. Lonkar, A. Sarkar, Experimental case studies for uncertainty quantification in structural dynamics, Probabilistic Eng. Mech. 24 (4) (2009) 473–492.
[26] S. Adhikari, On the quantification of damping model uncertainty, J. Sound Vib. 306 (1–2) (2007) 153–171.
[27] A. Kundu, S. Adhikari, Transient response of structural dynamic systems with parametric uncertainty, J. Eng. Mech. 140 (2) (2014) 315–331.
[28] P. Marek, J. Brozzetti, M. Gustar, I. Elishakoff, Probabilistic assessment of structures using Monte Carlo simulations, Appl. Mech. Rev. 55 (2) (2002) B31–B32.
[29] A. Olsson, G. Sandberg, O. Dahlblom, On latin hypercube sampling for structural reliability analysis, Struct. Saf. 25 (1) (2003) 47–68.
[30] M.D. Shields, J. Zhang, The generalization of latin hypercube sampling, Reliab. Eng. Syst. Saf. 148 (2016) 96–108.
[31] O. Araz, M.A. Shahraki, Optimal design of a novel enhanced inerter-based tuned mass damper in seismic-excited structures considering SSI effects, Adv. Eng. Softw. 217 (2026) 104162.
[32] O. Araz, Performance evaluation and optimization of nontraditional inerter-based tuned mass damper for seismic control of multi-story buildings considering SSI effects, in: Structures, Vol. 81, Elsevier, 2025, 110350.
[33] S. Prakash, R. Jangid, Optimum parameters of tuned mass damper-inerter for damped structure under seismic excitation, Int. J. Dyn. Control. 10 (5) (2022) 1322–1336.
[34] O. Araz, Optimal design of inerter-assisted series tuned mass dampers for seismic vibration control of multi-story buildings, Eng. Struct. 345 (2025) 121568.
[35] O. Araz, Effect of PGV/PGA ratio on seismic-induced vibrations of structures equipped with parallel tuned mass dampers considering SSI, in: Structures, Vol. 68, Elsevier, 2024, 107188.
[36] B. Besharatian, H.T. Riahi, R. Garcia, I. Hajirasouliha, Particle swarm optimization of friction tuned mass dampers subjected to ground motion records, Soil Dyn. Earthq. Eng. 172 (2023) 107995.
[37] A.Y. Pisal, R. Jangid, Vibration control of bridge subjected to multi-axle vehicle using multiple tuned mass friction dampers, Int. J. Adv. Struct. Eng. (IJASE) 8 (2) (2016) 213–227.
[38] B. Besharatian, H.T. Riahi, R. Garcia, I. Hajirasouliha, A practical optimisation method for friction tuned mass dampers in multi-storey buildings subjected to earthquake excitations, Soil Dyn. Earthq. Eng. 184 (2024) 108857.
[39] S. Adhikari, B. Pascual, The 'damping effect'in the dynamic response of stochastic oscillators, Probabilistic Eng. Mech. 44 (2016) 2–17.
[40] P. Billingsley, Probability and Measure, John Wiley & Sons, 2017.